The Neural Basis of Quantity Discrimination in Mice

Jikan Peng,[1,2,3] Dong Yang,[2,3] Chenshi Xu,[2,3,4] and Tian Xu [2,3,5,6,7, *]
[1]School of Medicine, Zhejiang University, Hangzhou, Zhejiang, China
[2]Key Laboratory of Growth Regulation and Translation Research of Zhejiang Province, School of Life Sciences, Westlake University, Hangzhou, Zhejiang, China
[3]Westlake Laboratory of Life Sciences and Biomedicine, Hangzhou, Zhejiang, China
[4]Fudan University, Shanghai, China
[5]Department of Genetics, Yale University School of Medicine, New Haven, USA
[6]Senior author
[7]Lead contact
*Correspondence: xutian@westlake.edu.cn

SUMMARY

Quantity discrimination is an ability of identifying preferable sizes or amounts of subjects, yet its mechanisms remain elusive. Here, we report that mice exhibit an innate quantity discrimination behavior for food amounts, consistent with the Weber-Fechner law. Inhibition of the Posterior Parietal Cortex (PPC), but not other cortex regions, disrupts this behavior. Two-photon analysis reveals that selected neurons with preferential activities or “Number Neurons” are detected at a given time; however, these neurons are not correlated with quantity discrimination behavior and alter their preferential identities over time. Furthermore, inhibition of other cortex regions with “Number Neurons” doesn’t affect quantity discrimination. Conversely, the PPC neuronal population changes synchronous firing levels, which correlates with quantity discrimination behavior and could be explained by a Neural Entropy model. Together, our study identifies a central role of the PPC in quantity discrimination, providing a neuronal population model of synchronous firing for quantity discrimination coding.

KEYWORDS

Quantity Discrimination, Posterior Parietal Cortex, Population Coding, Synchronous Firing, Neural Entropy.

INTRODUCTION

Quantity discrimination is an essential ability for human and animal survival. This ability enables individuals to judge different sizes or amounts of subjects for the preferable conditions. For example, human infants and chimpanzees choose a larger piece of cracker over a smaller one (Beran, 2001; Feigenson et al., 2002). Similarly, when presented with prey of different sizes, cats and cuttlefish select the larger one (Chacha et al., 2020; Yang and Chiao, 2016). Furthermore, when offered a choice between two sets of crackers with different amounts, human infants choose the set with more crackers (Feigenson et al., 2002). Similar behaviors were also observed in chimpanzees, dogs, monkeys, mongoose lemurs, sea lions, salamanders, and ungulate species (Abramson et al., 2011; Addessi et al., 2008; Krusche et al., 2010; Lewis et al., 2005; Miletto Petrazzini and Wynne, 2016; Schaffer et al., 2025; VanMarle et al., 2006). In addition to food, quantity discrimination behavior is also important when judging conspecifics, predators, and other environmental cues (Agrillo et al., 2008; Balestrieri et al., 2019; Gómez-Laplaza and Gerlai, 2010; Khatiwada and Burmeister, 2022; Lucon-Xiccato et al., 2017; Piffer et al., 2012; Sheardown et al., 2022). Therefore, quantity discrimination allows individuals to identify preferable conditions of sizes or amounts, which are crucial for obtaining resources, finding mates, or avoiding danger. Moreover, the presence of quantity discrimination behaviors from humans to fish suggests conserved mechanisms throughout evolution.

Brain imaging has identified potential cortex regions associated with quantity discrimination in humans when individuals were subjected to judging different numbers of dots or numerical symbols (Ansari et al.,

2005; Cantlon et al., 2006; Castelli et al., 2006; Chochon et al., 1999; Davis et al., 2009; Dehaene et al., 1998; Dehaene et al., 1996; Eger et al., 2003; Kaufmann et al., 2008; Piazza et al., 2006; Pinel et al., 2001; Zacharopoulos et al., 2021). In addition to the sensory cortex for processing inputs, the Prefrontal Cortex (PFC) and the Posterior Parietal Cortex (PPC) were identified in these fMRI studies for quantity discrimination. In addition to brain imaging studies, electrophysiological recording in monkeys has also identified neuronal activities within the PFC, the PPC, as well as the Anterior Inferior Temporal Cortex (aITC), when animals were trained to recognize images with the same number of dots (Nieder et al., 2002; Nieder and Miller, 2004; Sawamura et al., 2002). Moreover, these electrophysiological studies identified individual neurons in these three regions exhibiting activities preferentially tuned towards a given number of dots (Nieder et al., 2002; Nieder and Miller, 2004; Sawamura et al., 2002). Thereafter, it has been proposed that these specific neurons, or the "Number Neurons", represent an abstract code for numbers (Nieder, 2016; Nieder et al., 2006; Nieder and Miller, 2003).

Here, we report the establishment of a food-based assay for quantity discrimination in the model organism, the mouse. Furthermore, we have identified the functional involvement of the PPC in quantity discrimination through viral-mediated reversible chemogenetic neural inhibition. Finally, we have analyzed neuronal activities in the PPC using two-photon imaging during quantity discrimination. Our analysis does not support the "Number Neurons" coding hypothesis, and instead, reveals that the PPC neuronal population exhibits changes in synchronous firing levels, which correlates with quantity discrimination behavior.

RESULTS

A Food-based Assay Reveals Quantity Discrimination Behavior in Mice

We investigated whether mice have an innate capacity of quantity discrimination when presented with different amounts of food. In the food-based assay, individual naïve adult mice were introduced into an open field arena containing designated amounts of food in the two opposing corners (Figure 1A and 1B; STAR Methods). The foraging movement of each animal was continuously monitored for one hour and the accumulative time each animal spent within the specific zone with the different amount of food was analyzed. A representative example of the foraging behavior was illustrated in Figure 1C (Figure S1). When presented with 20g versus 80g of food in the assay, significant disparities were observed for the times that individual mice spent in different foraging zones, resulting in measurements of 20.17 ± 2.13% (Mean ± SEM) and 67.34 ± 2.80%, respectively (Figure 1D, N=6; p=9.88e-04, Paired t-test). Moreover, the amounts of food consumed from the 80g container was approximately twice that from the 20g container (Figure S2A, N=6; 20g: 0.76 ± 0.09g; 80g: 1.77 ± 0.09g; p=5.74e-04, Paired t-test). No disparity was observed when equal amounts of food were presented in the assay (Figure 1D and S2A, N=6; 40g: 44.39 ± 3.09%; 40g: 44.30 ± 3.97%; p=9.90e-01, Paired t-test). In addition to the C57BL/6J strain, the 129 and the BALB/c strains of mice exhibited similar behavior (Figure 1E and S2B; 129: N=6, p=4.75e-03, 20g: 35.51 ± 2.44%; 80g: 58.70 ± 2.48%; BALB/c: N=6, p=4.36e-04, 20g: 34.53 ± 1.83%; 80g: 56.06 ± 0.97%; Paired t-test). Finally, the quantity discrimination behavior was also observed when additional different amounts of food were presented (Figure 1F and S3). These results revealed that mice can distinguish different amounts of food and show a preference towards more food, exhibiting a true quantity discrimination behavior. Furthermore, the quantity discrimination for amounts of food is an innate behavior in mice without training, facilitating and simplifying future mechanistic studies.

In addition to brain imaging studies, the relationship between the different numbers or ratios of dots and the discriminating ability has been examined in humans of different ages (Halberda and Feigenson, 2008). These studies revealed that human's ability to discriminate dots follows the Weber-Fechner law, which is a general principle in behavioral science describing the relationship between the intensity of the physical stimuli and the perceived strength of these stimuli (Fechner, 1860; Weber, 1834). We therefore examined the relationship between different amounts or ratios of food and the quantity discrimination behavior in mice and confirmed that food quantity discrimination in mice also follows the Weber-Fechner law (Figure 1F,

S2A, and S3; Table S1). The Weber-Fechner law also specifies a threshold for discriminating distinct stimulus intensities, known as the Weber fraction indicating the strength of perception ability (Fechner, 1860; Weber, 1834). Our experiments revealed a Weber fraction value of 0.37 for food quantity discrimination in mice (Figure 1F, S2A, and S3). Together, these results indicate that the food quantity discrimination behavior in mice is similar to the ability to discriminate dots in humans and with the ability comparable to 3 year-old humans (Halberda and Feigenson, 2008).

Visual Input Is Required for Food Quantity Discrimination in Mice

We then explored the sensory modality influencing the behavior of food quantity discrimination in mice. We first assessed the contribution of olfactory sensation by inducing temporary anosmia with a chemical agent (STAR Methods). Despite successful induction of olfactory anosmia (Figure S4), the food quantity discrimination behavior was not disrupted in mice (Figure 1G and S2C, N=6; 20g: 25.36 ± 3.11%; 80g: 68.22 ± 3.44%; p=1.09e-03, Paired t-test). Subsequently, we evaluated the role of tactile sensation by removal of tactile bristles (Petersen, 2019) and found that the food quantity discrimination behavior maintained (Figure 1G and S2C, N=6; 20g: 23.04 ± 2.41%; 80g: 69.12 ± 2.17%; p=1.48e-04, Paired t-test).

In contrast, disruption of visual sensation via surgical ablation of retinal ganglion fibers resulted in a loss of the food quantity discrimination in mice (Figure 1G and S2C, N=6; 20g: 41.77 ± 4.70%; 80g: 42.51 ± 4.54%; p=9.38e-01, Paired t-test). This observation was further confirmed by experiments with visually compromised mice, including FVB adults with retinal detachment (Figure 1G and S2C, N=6; 20g: 41.63 ± 5.65%; 80g: 43.35 ± 4.55%; p=8.72e-01, Paired t-test) and $Arf^{FL/+}$ transgenic animals with congenital blindness (Figure 1G and S2C, N=6; 20g: 43.74 ± 3.09%; 80g: 45.82 ± 1.70%; p=6.49e-01, Paired t-test). To underscore the importance of visual cues in food quantity discrimination, we conducted a visual illusion experiment with wild-type animals, in which a plastic block was buried in food in the container with less food, visually aligning it with the container with more food (40g with block, 80g without block; STAR Methods). Consistent with experiments of damaged visual system, visual illusion disrupted the food quantity discrimination (Figure 1D, 1G, S2A and S2C, N=6; 40g: 40.86 ± 4.15%; 80g: 45.72 ± 2.21%; p=4.11e-01, Paired t-test). These findings revealed that visual input is critical for food quantity discrimination in mice.

The PPC Is Required for Quantity Discrimination

We then investigated which brain regions might be functionally required for quantity discrimination in mice. As fMRI imaging and electrophysiological recording in humans and monkeys have revealed associated activities in several cortex regions with quantity discrimination (Ansari et al., 2005; Cantlon et al., 2006; Chochon et al., 1999; Dehaene et al., 1998; Dehaene et al., 1996; Nieder et al., 2002; Nieder and Miller, 2004; Pinel et al., 2001; Sawamura et al., 2002), we examined whether the PPC is functionally required for quantity discrimination for food in mice using viral-mediated reversible chemogenetic neural inhibition (Figure S5; STAR Methods). We found that inhibition of the PPC eliminated the food quantity discrimination behavior in mice (Figure 2A and S2D, N=6; 20g: 43.48 ± 3.93%; 80g: 43.47 ± 4.18%; p=9.99e-01, Paired t-test). In contrast, inhibition of the mouse equivalent of aITC, the Postrhinal Association Cortex (POR), did not disrupt this quantity discrimination behavior (Figure 2A and S2D, N=6; 20g: 24.37 ± 1.79%; 80g: 63.28 ± 1.30%; p=1.76e-05, Paired t-test). To discern if the disruption of the PPC activity might impact visual sensory function, we conducted a novel object recognition test and confirmed that visual sensory activity was unaffected by the PPC inhibition (Figure S6; STAR Methods). Together, our findings in mice provided the first evidence that the PPC is functionally required for quantity discrimination.

No "Number Neurons" for Quantity Discrimination

In the electrophysiological studies of monkeys, specific neurons with preferential activities for different number of dots, or the "Number Neurons", were identified in three cortical regions: the PPC, the POR/aITC, and the PFC (Nieder et al., 2002; Nieder and Miller, 2004; Sawamura et al., 2002). However, our

experiments revealed that inhibition of the POR/aITC did not disrupt quantity discrimination in mice (Figure 2A). Among the three cortex regions, 30% of the recorded neurons in the PFC are the “Number Neurons”, which is much higher than 10% and 5% detected in the PPC and the POR/aITC, respectively (Nieder and Miller, 2004). Therefore, to further investigate whether the “Number Neurons” are involved in quantity discrimination, we inhibited the PFC, which has the most “Number Neurons”, and found that this inhibition also did not disrupt quantity discrimination behavior (Figure 2A, S2D and S5, N=6; 20g: 25.75 ± 2.23%; 80g: 59.15 ± 3.19%; p=1.06e-03, Paired t-test; STAR Methods). These findings suggested that the “Number Neurons” may not be required for quantity discrimination.

As the “Number Neurons” were also identified in the PPC (Nieder and Miller, 2004; Sawamura et al., 2002), we decided to conduct a detail examination of the neuronal activities in the PPC during quantity discrimination in mice using two-photon imaging technology. This technology allows one to continuously monitor the activities of more than hundred neurons in each freely moving animal over extended periods (Zong et al., 2017). Briefly, we virally expressed the calcium indicator GCaMP6f in the PPC and recorded neuronal activities within layer II/III of the PPC during the food quantity discrimination assay using two-photon microscopy (Figure 2B and Figure S7; STAR Methods) (Kaszas et al., 2021). The activities of 7,378 neurons across 48 mice were recorded, and the data were processed following standard procedures and both firing rate and firing magnitude for each neuron were calculated (Figure 2C, S8, and S9; Table S2; STAR Methods) (de Vries et al., 2020; Giovannucci et al., 2019; Pnevmatikakis and Giovannucci, 2017). We did detect about 10% of the PPC neurons showing preferential activities towards either the 20g or 80g of food at a given time (Figure 2D and S10), which is very similar to the results from the electrophysiology studies in monkeys (Nieder and Miller, 2004; Sawamura et al., 2002). However, when the same neurons were followed at different periods, they had altered their preferential activities toward the different food amounts (Figure 2D, S10, and S11). In other words, the “Number Neurons” had altered their preferential identities. Finally, we examined the “Number Neurons” phenomenon when the animals were presented with the equal amounts of food (20g versus 20g). We found that neurons with preferential activities were still detected at a given time and again such preferential activities changed over time (Figure 2E, S10, and S11). Together, these results indicated that there are no true “Number Neurons” and argue against the “Number Neuron” coding hypothesis.

The Levels of Synchronous Firing in the PPC Neuronal Population Predict Quantity Discrimination Behavior

As selected neurons with preferential activities fail to explain quantity discrimination, we analyzed the population of the PPC neurons for potential activity pattern predicting quantity discrimination behavior. First, we found that there is no significant difference in the number of firing neurons or the magnitude of their firing when the animals were presented with different amounts of food (Figure S12 and Table S2; STAR Methods). We then analyzed the pattern of synchronous firing of the PPC neuronal population during quantity discrimination (STAR Methods). This analysis revealed that significant number of the PPC neurons exhibit synchronous firing, with a Jaccard Index value as high as 0.7 (Figure 3A and Table S2). The average duration of the synchronous firing is 1.95 ± 0.02 seconds (Table S2 and Figure S13). Furthermore, we discovered that all the recorded PPC neurons are activated during quantity discrimination and are participated in synchronous firing (Figure S14; STAR Methods). Excitingly, we discovered that the levels of synchronous firing of the PPC neuronal population are changed when animals were presented with different amounts of food (Table 1). Specifically, when the animals were presented with either 20g or 80g of food, the corresponding levels of synchronous firing were 23.40 ± 1.98% and 17.73 ± 1.77%, respectively (Table 1, Figure 3B and S15, N=6; p=0.00e-00, Mann-Whitney U test). In contrast, when the animals were presented with the same amount of food (20g versus 20g), the level of synchronous firing remained the same (Table 1, Figure 3C and S15, N=6; 20g: 23.35 ± 1.38%; 20g: 23.26 ± 1.26%; p=6.94e-01, Mann-Whitney U test). When additional different amounts of food were examined (40g, 60g, 70g, and 90g), we discovered that the levels of synchronous firing inversely correlated with the amounts of food (Table 1, Figure 3D and S15). Together, these data revealed that the PPC neuronal population exhibits significant

levels of synchronous firing and the levels of synchronous firing correlate with the quantity discrimination behavior.

It is intriguing how the levels of synchronous firing in the PPC could code the information for quantity discrimination. The fundamental elements of synchronous firing are the firing or the resting status of individual neurons, which is very similar to the on or the off status of the transistors on the computer chip (Tsai et al., 2023). The quantity information or other contents coded by the binary statuses of the transistors on a chip is measured by Shannon's Entropy (Figure 4A; STAR Methods) (Shannon, 1948). By analogy, we proposed a Neural Entropy model to calculate the levels of synchronous firing in the PPC or in any given population of neurons (Figure 4B; STAR Methods). Specifically, the firing or the resting status of each neuron behaves as a binary coding unit. The aggregation of pairwise synchronous firing for all neurons in the population or the level of synchronous firing could be calculated accordingly following the Neural Entropy model (Figure 4B; STAR Methods). Using the recorded data of neuronal activities in the PPC during quantity discrimination, we calculated the Neural Entropy values for the 20g or 80g of food quantity discrimination to be 0.14 ± 0.01 or 0.45 ± 0.01 bits, respectively, which is consistent with the quantity discrimination behavior (Figure 4B, N=6; p=4.72e-06, Paired t-test). Furthermore, the Neural Entropy calculation based on the levels of synchronous firing for the other different amounts of food also resulted in distinctive values consistent with the outcomes of the behavior (Figure 4B; Figure S16). Together, these findings indicated that the levels of synchronous firing in the PPC predicts the quantity discrimination behavior, whose values could be measured by the Neural Entropy model.

DISCUSSION

Quantity discrimination enables individuals to identify preferable sizes or amounts of subjects, such as food, that are essential for animal survival. Here, we have established the first food-based assay to study quantity discrimination behavior in a model organism. Different strains of mice display an innate quantity discrimination ability for different amounts of food. Our analysis revealed that this ability for food amounts relies on the stimulus input from visual perception. Furthermore, the relationship between stimulus intensity of food amounts and quantity discrimination in mice follows the Weber-Fechner law, which is consistent with the results in humans for identifying different numbers or dots (Fechner, 1948; Halberda and Feigenson, 2008; Weber, 1834). Compared to humans, monkeys, and crows, which have been used to study quantity discrimination in the past, the mouse as a model organism offers many advantages for experimental manipulation and mechanistic exploration. Finally, different from discriminating dot numbers or sound beats in the past studies, quantity discrimination for different amounts of food is an innate behavior without training. Such an innate assay offers unique advantages in reducing the complexity and confounding factors introduced by learning and training.

Multiple cortex regions have been previously suggested to be involved in quantity discrimination through fMRI imaging and electrophysiological recording for discriminating dot numbers or numerical symbols in humans and monkeys (Ansari et al., 2005; Cantlon et al., 2006; Castelli et al., 2006; Chochon et al., 1999; Davis et al., 2009; Dehaene et al., 1998; Dehaene et al., 1996; Eger et al., 2003; Kaufmann et al., 2008; Nieder et al., 2002; Nieder and Miller, 2004; Piazza et al., 2006; Pinel et al., 2001; Sawamura et al., 2002; Zacharopoulos et al., 2021). Using chemical genetic inhibition experiments, we have now shown that inhibition of the PPC, but not the PFC or the POR/aITC, blocks food quantity discrimination in mice. Additionally, our companion study has shown that patients with surgery involved in the PPC fail in quantity discrimination and there is a genetic association between the PPC and intelligence for quantity discrimination (unpublished) (Yang et al., 2025). Overall, our findings have, for the first time, identified that the PPC is functionally required for quantity discrimination. Recent studies have shown that the PPC is also involved in navigation decision (Carandini and Churchland, 2013; Hanks and Summerfield, 2017; Lyamzin and Benucci, 2019). Specifically, mice were trained for navigation decision in discriminative responses to images of dots, stripes, or different sound tones (Ashwood et al., 2022; Driscoll et al., 2017; Goard et al., 2016; Green et al., 2023; Harvey et al., 2012; Hwang et al., 2017; Kuan et al., 2024; Lee et al., 2022;

Minderer et al., 2019; Morcos and Harvey, 2016; Orlandi et al., 2023; Pho et al., 2018; Posner et al., 2022; Sheng et al., 2024; Song et al., 2017; Wang et al., 2024; Zhong et al., 2019). Together, our work and the previous studies indicate that the PPC is responsible for discriminative decisions.

The electrophysiological recording of monkeys for recognizing the number of dots identified the existence of specific neurons exhibiting activities preferential towards specific numbers of dots, which led to the hypothesis that these "Number Neurons" represent an abstract code for numbers or quantity discrimination (Nieder, 2016; Nieder et al., 2006; Nieder et al., 2002; Nieder and Miller, 2003, 2004; Sawamura et al., 2002). However, multiple lines of evidence from this work and the navigation decision studies are against the existence of such "Number Neurons" and their role in quantity discrimination. First, our results showed that inhibition of the PFC or the POR/aITC, two regions containing "Number Neurons" (Nieder et al., 2002; Nieder and Miller, 2004; Sawamura et al., 2002), did not affect quantity discrimination. Second, when the animals were presented with the equal amounts of food, neurons with different preferential activities were still detected. Third, and more importantly, our experiments revealed that the neurons with preferential activities alter their preferential identities as two-photon imaging continuously monitored the activities for the same neurons over time. Similar results were also reported in the navigation decision studies, in which two-photon analysis revealed that the neurons in the PPC with preferential activities were detected at a given time and such preferential activities altered over time (Driscoll et al., 2017; Lee et al., 2022; Zhong et al., 2019). Therefore, there is no true "Number Neurons". Furthermore, the "Number Neurons" coding hypothesis also has shortcomings in theoretical consideration. First, if it requires a special group of "Number Neurons" to code for each number, a vast number of neurons are needed to code for many numbers. By contrast, we and others have found that the levels of synchronous firing or the states of the PPC neuronal population discriminates different quantity or navigation conditions. In other words, the PPC functions by determining differences in quantities or conditions in the given situations, which could be applied to numerous settings. The most unsettlingly issue is the "Number Neurons" coding hypothesis does not explain which number is bigger, which is essential to quantity discrimination in determining the preferable condition(s) for animal survival. Together, both experimental evidence and theoretical considerations do not support the "Number Neurons" coding hypothesis.

To elucidate the underlying neural basis for quantity discrimination, we have recorded and analyzed the activities of individual neurons in the PPC neuronal population using two-photon microscopy. Our analysis revealed that there is no significant difference in either the number of firing neurons or the firing magnitude when the animals were presented with different amounts of food. Instead, we found that all neurons in the PPC exhibit activities during quantity discrimination and significant number of them display synchronous firing. Interestingly, we have discovered that the levels of synchronous firing of the PPC neuronal population correlate with the quantity discrimination behavior. Therefore, our results indicate that the coding of the PPC for quantity discrimination does not depend on the number of firing neurons, the firing magnitude, or special neurons with preferential activities, but rather on the levels of synchronous firing of the PPC neuronal population. The fundamental elements of synchronous firing are the firing and resting binary statuses of individual neurons in a neuronal population. Binary coding systems have been utilized throughout human history, including the Chinese Bagua, Africa Ifa, Braille for visually impaired, and the transistors in computer chips (Alamu et al., 2013; Tsai et al., 2023). The information content for the computer chip(s) is coded by the binary statues of the collection of the transistors and calculated by Shannon's Entropy (Shannon, 1948). In analogy, we have proposed a Neural Entropy model for calculating the information content of synchronous firing of a neuronal population and discovered that the Neural Entropy values of synchronous firing of the PPC neuronal population could predict the quantity discrimination behavior. It is intriguing to consider whether similar coding system operates in other neuronal populations of the brain. Finally, it is fascinating to speculate whether forthcoming studies of the coding and energy strategies of the PPC could facilitate the design of future chips and computers.

RESOURCE AVAILABILITY

Lead contact

Further information and requests for resources and reagents should be directed to and will be fulfilled by the lead contact, Tian Xu (xutian@westlake.edu.cn).

Materials availability

Correspondence and requests for materials should be addressed to the lead contact.

Data and code availability

All data are available in this manuscript. Codes for behavior analysis or two-photon imaging analysis are available from the authors on request.

ACKNOWLEDGMENTS

We thank Lijun Xiang and Hongyan Yang for technical assistance and the Xu lab members for discussion. This study was supported in part by the grants to TX including National Natural Science Foundation of China (U21A20201), Key Laboratory of Growth Regulation and Translational Research of Zhejiang Province (2020E10027), the Science Technology Department of Zhejiang Province (2021ZY1019, 2022ZY1005), Zhejiang Leading Innovative and Entrepreneur Team Introduction Program (2018R01003), and Westlake Laboratory of Life Sciences and Biomedicine (202208011). JKP and CSX are supported by Westlake University Predoctoral Fellowship. TX is grateful to Yale and HHMI for more than two decades of support.

AUTHOR CONTRIBUTIONS

Conceptualization, JKP and TX; Methodology, JKP; Investigation, JKP and CSX; Visualization, JKP and DY; Funding acquisition, TX; Project administration, TX; Supervision, TX; Writing – original draft, JKP and TX; Writing – review & editing, JKP and TX.

DECLARATION OF INTERESTS

Authors declare that they have no competing interests.

SUPPLEMENTAL INFORMATION

Document S1. Tables S1–S2.
Table S1. The amounts of food and their ratios in the quantity discrimination assay, related to Figure 1
Table S2. Two-photon imaging experiments, related to Figure 3

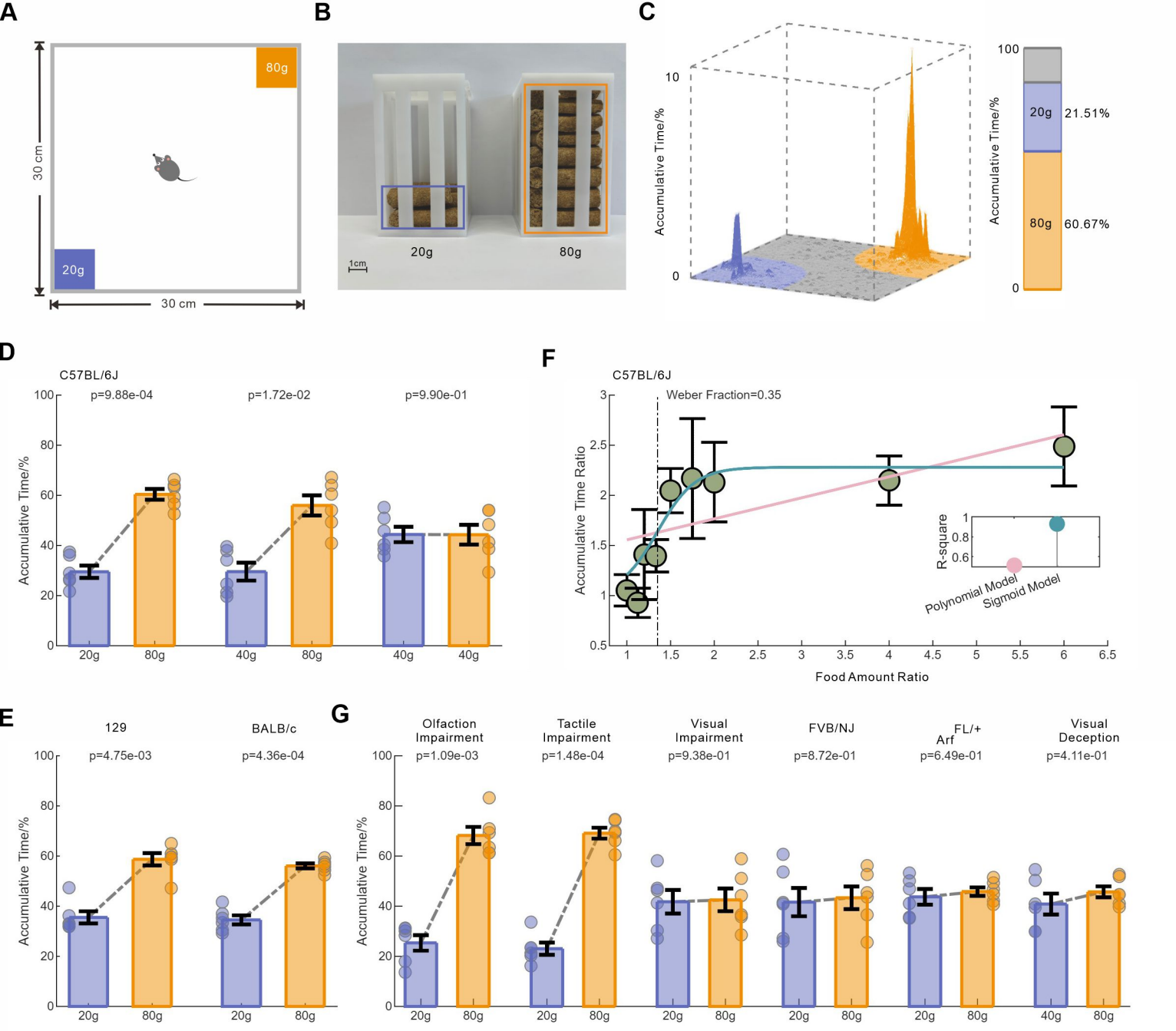
A
80g
30 cm
20g
30 cm
B
20g
80g
1cm
C
Accumulative Time/%
10
0
100
20g 21.51%
80g 60.67%
0
D
C57BL/6J
p=9.88e-04
p=1.72e-02
p=9.90e-01
Accumulative Time/%
20g
80g
40g
80g
40g
40g
E
129
BALB/c
p=4.75e-03
p=4.36e-04
Accumulative Time/%
20g
80g
20g
80g
F
C57BL/6J
Weber Fraction=0.35
Accumulative Time Ratio
Food Amount Ratio
R-square
Polynomial Model
Sigmoid Model
G
Olfaction Impairment
p=1.09e-03
Tactile Impairment
p=1.48e-04
Visual Impairment
p=9.38e-01
FVB/NJ
p=8.72e-01
FL/+ Arf
p=6.49e-01
Visual Deception
p=4.11e-01
Accumulative Time/%
20g
80g
20g
80g
20g
80g
20g
80g
20g
80g
40g
80g

Figure 1. Quantity Discrimination for Food Amounts in Mice

(A) Schematic representation of different amounts of food in an open arena in a food-based quantity discrimination assay.

(B) Representative food containers holding either 20g or 80g of food.

(C) Tracking map illustrating the percentage of time the animal spent in each foraging zone (20g versus 80g).

(D-E) Quantity discrimination behavior for different ratios of food amounts in the C57BL/6J (D), 129 and BALB/c (E) mice.

(F) Quantity discrimination behavior for food amounts in mice follows the Weber-Fechner law. The relationship of the food amount ratio versus the accumulative time ratio fits with either the sigmoid (green line) or the polynomial (purple line) model. The corresponding R-square values indicate model fitness, while the estimated Weber Fraction is marked by the dotted line.

(G) Quantity discrimination behavior following block of specific sensory inputs including chemical-induced olfactory anosmia, tactile sensory deprivation by whisker removal, or visual impairment due to crushing of optic nerves, retinal detachment, blindness, or visual deception of food amount.

Paired t-test. Bars indicate Mean ± SEM. Dots manifest data from individual mice (D, E, and G). See also Table S1 and Figure S1-4.

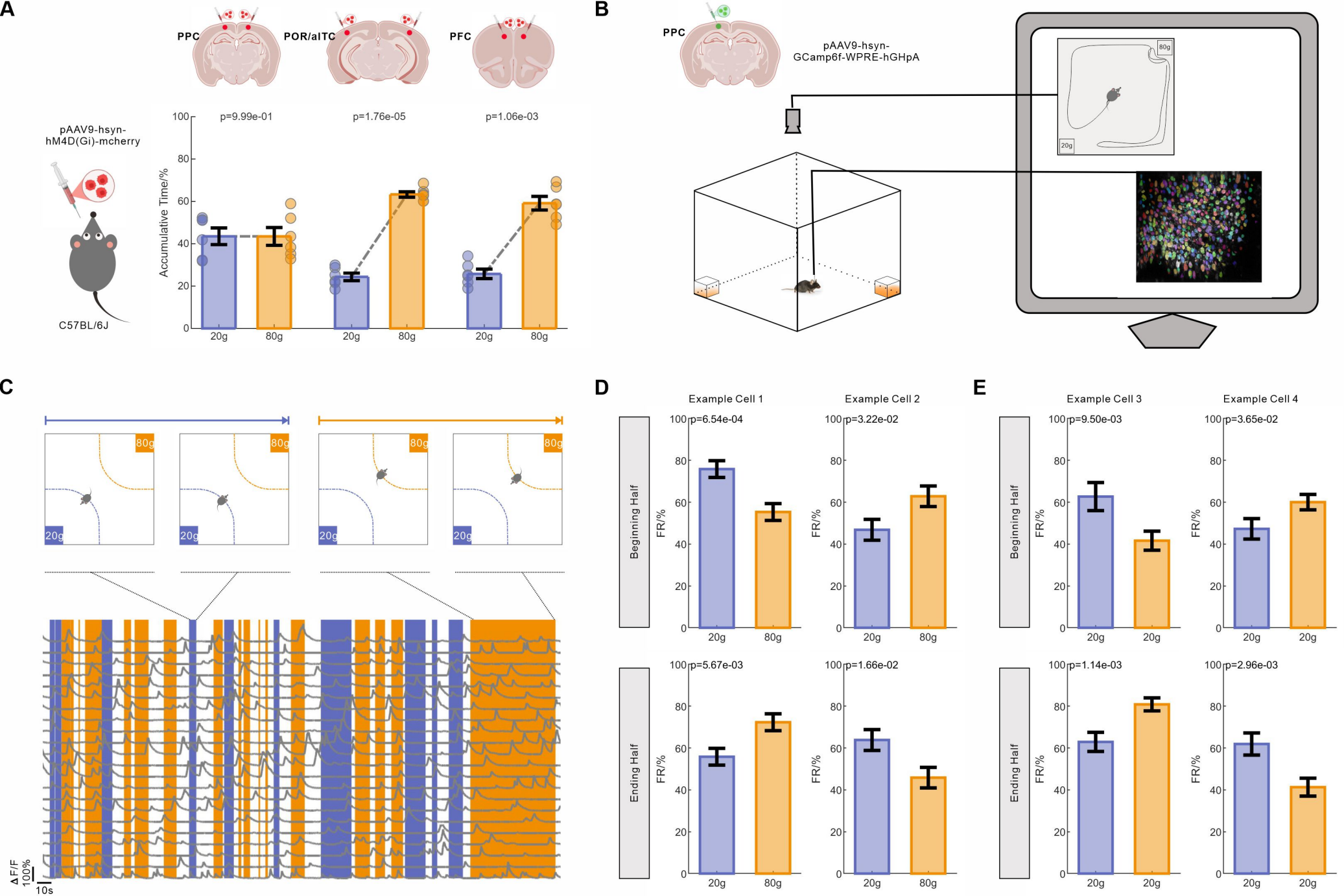
A
PPC
POR/aITC
PFC
pAAV9-hsyn-
hM4D(Gi)-mcherry
C57BL/6J
p=9.99e-01
p=1.76e-05
p=1.06e-03
Accumulative Time/%
20g
80g
B
PPC
pAAV9-hsyn-
GCamp6f-WPRE-hGHpA
C
ΔF/F
100%
10s
D
Example Cell 1
Example Cell 2
Beginning Half
Ending Half
FR/%
p=6.54e-04
p=3.22e-02
p=5.67e-03
p=1.66e-02
E
Example Cell 3
Example Cell 4
p=9.50e-03
p=3.65e-02
p=1.14e-03
p=2.96e-03

341 **Figure 2. The Involvement of the PPC for Quantity Discrimination**
342 (A) Quantity discrimination behavior in mice following the inhibition of neuronal activities in the PPC, the
343 POR/aITC, or the PFC.

344 (B) Two-photon imaging analysis for neuronal activities in layer II/III of the PPC during the quantity
345 discrimination assay.

346 (C) Representative calcium signals from the PPC neurons are shown, alongside illustration of foraging
347 zone-visit events.

348 (D) Altered preferential activities of two typical neurons in the PPC during the quantity discrimination assay
349 for 20g versus 80g of food at either the beginning (upper) or the ending half (lower).

350 (E) Preferential activities of two typical neurons in the PPC during the quantity discrimination assay for 20g
351 versus 20g of food at either the beginning (upper) or the ending half (lower).

352 Unpaired t-test (D, E). Bars indicate Mean ± SEM; Dots manifest individual data. See also Figure S2, and
353 Figure S5-11.

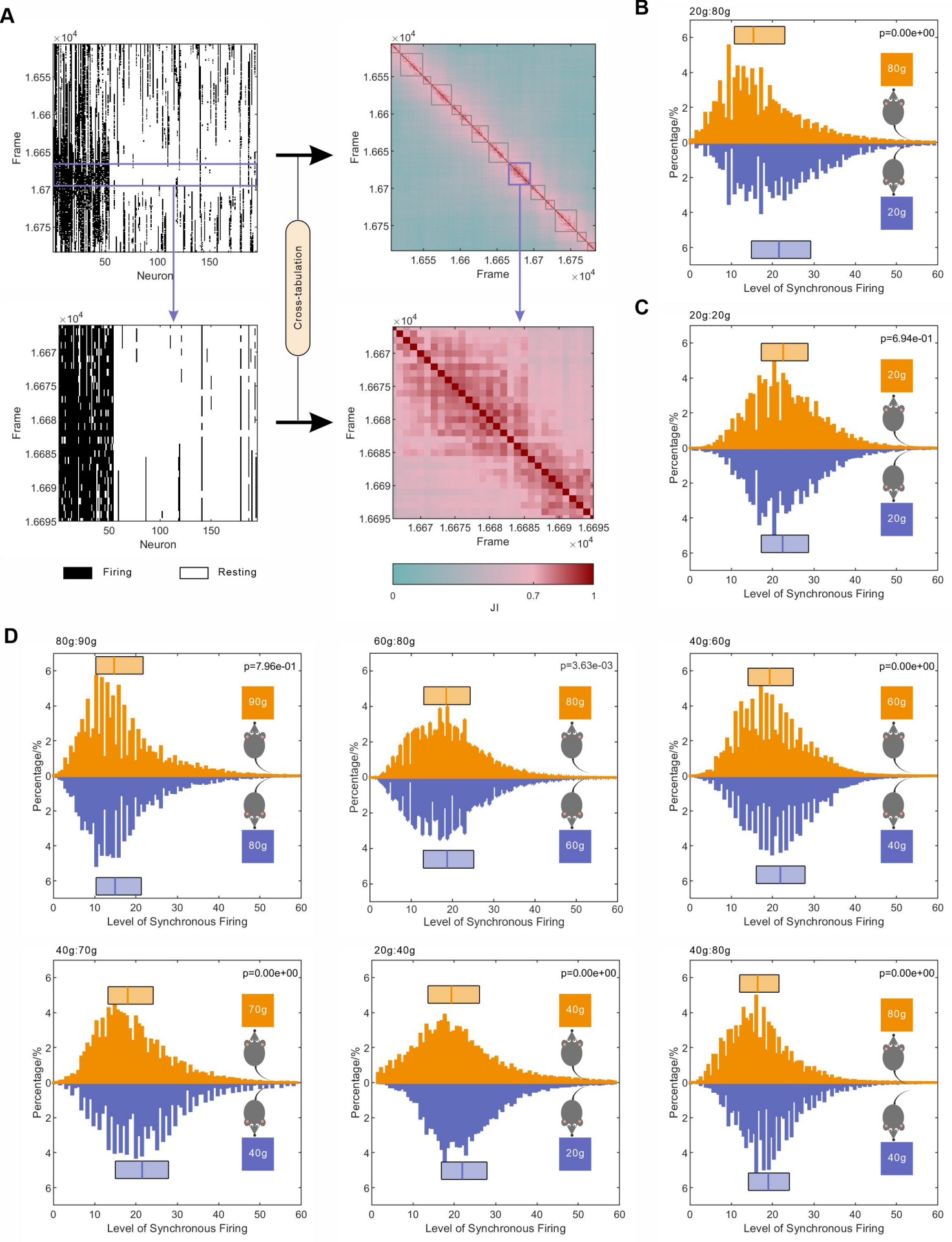
A
Frame
Neuron
Cross-tabulation
Firing
Resting
JI
B
20g:80g
p=0.00e+00
80g
20g
Percentage/%
Level of Synchronous Firing
C
20g:20g
p=6.94e-01
20g
20g
D
80g:90g
p=7.96e-01
90g
80g
60g:80g
p=3.63e-03
80g
60g
40g:60g
p=0.00e+00
60g
40g
40g:70g
p=0.00e+00
70g
40g
20g:40g
p=0.00e+00
40g
20g
40g:80g
p=0.00e+00
80g
40g

Figure 3. Synchronous Firing in the PPC Neuronal Population during Quantity Discrimination

(A) The activation patterns of the PPC neuronal population at any given time (left), and the synchronous firing of a group of neurons (right, gray or blue blocks), as indicated by the Jaccard Index (JI) calculation (STAR Methods)

(B-D) The levels of synchronous firing in the PPC neuronal population during quantity discrimination assay for 20g versus 80g of food (B), 20g versus 20g of food (C), or additional different amounts of food (D). the original distributions are represented by median values and interquartile ranges. Mann-Whitney U test. See also Table 1, Table S2, and Figure S12-15.

A

Shannon Entropy for Quantity Memory in Computer

A Transistor

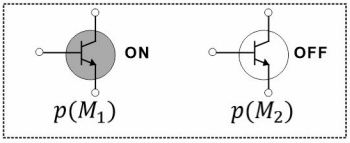

$$H(M) = \sum_{i=1}^{2} p(M_i) log_2^{1/p(M_i)}$$

A Byte of 8 Transistors

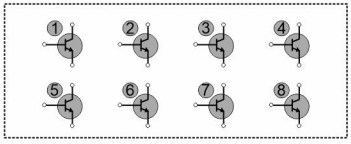

$$H = \sum_{M=1}^{8} \sum_{i=1}^{2} p(M_i) log_2^{1/p(M_i)}$$

A Population of Transistors

$$H = \sum_{M=1}^{S} \sum_{i=1}^{2} p(M_i) log_2^{1/p(M_i)}$$

S: The Number of Transistors in Population

B

Neural Entropy for Quantity Discrimination in Brain

A Neuron

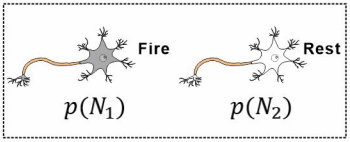

$$H(N) = \sum_{i=1}^{2} p(N_i) log_2^{1/p(N_i)}$$

A Pair of Neurons

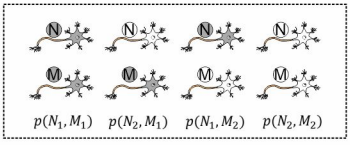

$$H(N, M) = \sum_{j=1}^{2} \sum_{i=1}^{2} p(N_j, M_i) log_2^{1/p(N_j, M_i)}$$

A Population of Neurons

$$N(X) = \frac{p(X)}{C_S^2} \sum_{N=1}^{S-1} \sum_{M=N+1}^{S} H(N, M)$$

S: The Number of Neurons in Population
p(X): Probability at Condition X
C_S^2: Pairs of Synchronous Firing Neurons

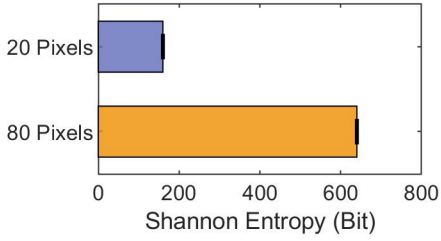

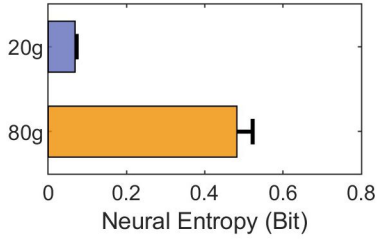

Figure 4. Neural Entropy Model for Quantity Discrimination

(A) Calculation of Shannon Entropy for a single memory transistor, a Byte of eight transistors, and a population of transistors on a chip. The specified entropy values for encoding gray images with either 20 or 80 pixels.

(B) Calculation of Information content for a single neuron, a pair of neurons, and a population of neurons in the PPC. The Neural Entropy values for synchronous firing are calculated from the neuronal activities of the PPC during quantity discrimination for 20g versus 80g of food. See also Figure S16.

369 **Table 1. Levels of synchronous firing during quantity discrimination**

Amounts of Food (g/g)	Levels of Synchronous Firing (%)[a]	Statistical Significance (p-value)[b]
20:20	23.35 ± 1.38 : 23.26 ± 1.26	6.94e-01
80:90	16.84 ± 1.19 : 16.43 ± 1.25	7.96e-01
60:80	21.11 ± 1.53 : 18.62 ± 1.43	3.63e-03
40:60	22.96 ± 1.19 : 19.96 ± 1.43	0.00e+00
40:70	22.29 ± 0.23 : 19.54 ± 0.26	0.00e+00
20:40	23.21 ± 0.51 : 20.94 ± 0.42	0.00e+00
40:80	19.86 ± 1.20 : 17.50 ± 1.11	0.00e+00
20:80	23.40 ± 1.98 : 17.73 ± 1.77	0.00e+00

370 [a] Values are presented as Mean ± SEM.
371 [b] Mann-Whitney U test.

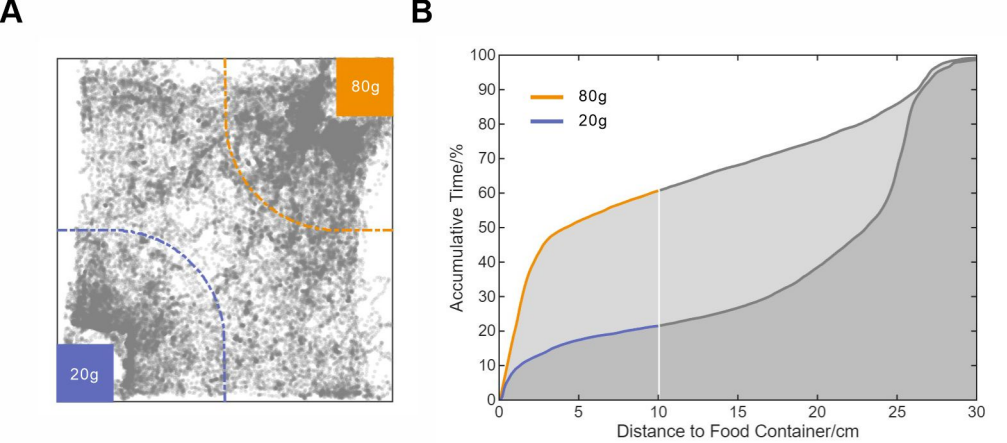
A
80g
20g
B
80g
20g
Accumulative Time/%
Distance to Food Container/cm
0
10
20
30
40
50
60
70
80
90
100
0
5
10
15
20
25
30

Figure S1. Tracking Map in the Assay, Related to Figure 1

(A-B) Representative tracking map illustrating the percentage of time the mouse spent in each foraging zone (20g versus 80g, A), along with its proximity to the food containers (B).

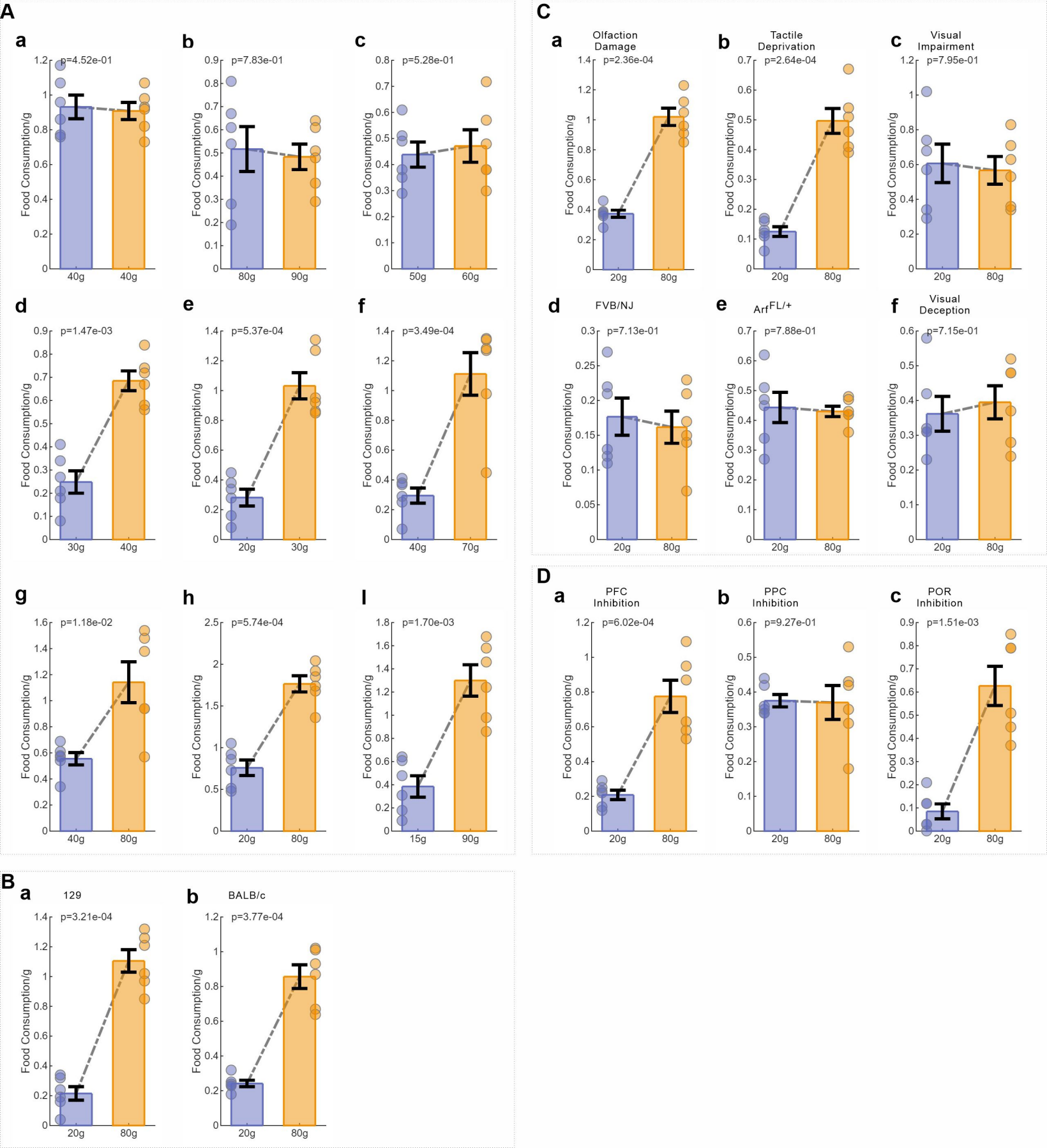
A
a
p=4.52e-01
40g
40g
b
p=7.83e-01
80g
90g
c
p=5.28e-01
50g
60g
d
p=1.47e-03
30g
40g
e
p=5.37e-04
20g
30g
f
p=3.49e-04
40g
70g
g
p=1.18e-02
40g
80g
h
p=5.74e-04
20g
80g
I
p=1.70e-03
15g
90g
B
a
129
p=3.21e-04
20g
80g
b
BALB/c
p=3.77e-04
20g
80g
C
a
Olfaction Damage
p=2.36e-04
20g
80g
b
Tactile Deprivation
p=2.64e-04
20g
80g
c
Visual Impairment
p=7.95e-01
20g
80g
d
FVB/NJ
p=7.13e-01
20g
80g
e
ArfFL/+
p=7.88e-01
20g
80g
f
Visual Deception
p=7.15e-01
20g
80g
D
a
PFC Inhibition
p=6.02e-04
20g
80g
b
PPC Inhibition
p=9.27e-01
20g
80g
c
POR Inhibition
p=1.51e-03
20g
80g
Food Consumption/g

375 **Figure S2. Food Consumption in the Assay, Related to Figure 1 and 2**

376 (A) Food consumption by C57BL/6J mice in different quantity discrimination assays.

377 (B) Food consumption by 129 and BALB/c mice.

378 (C) Food consumption by C57BL/6J mice in sensory input deprivation experiments.

379 (D) Food consumption by C57BL/6J mice in the experiments of inhibition of the PFC, the PPC, or the
380 POR/aITC.

381 Paired t-test. Bars indicate Mean ± SEM. Dots manifest individual data.

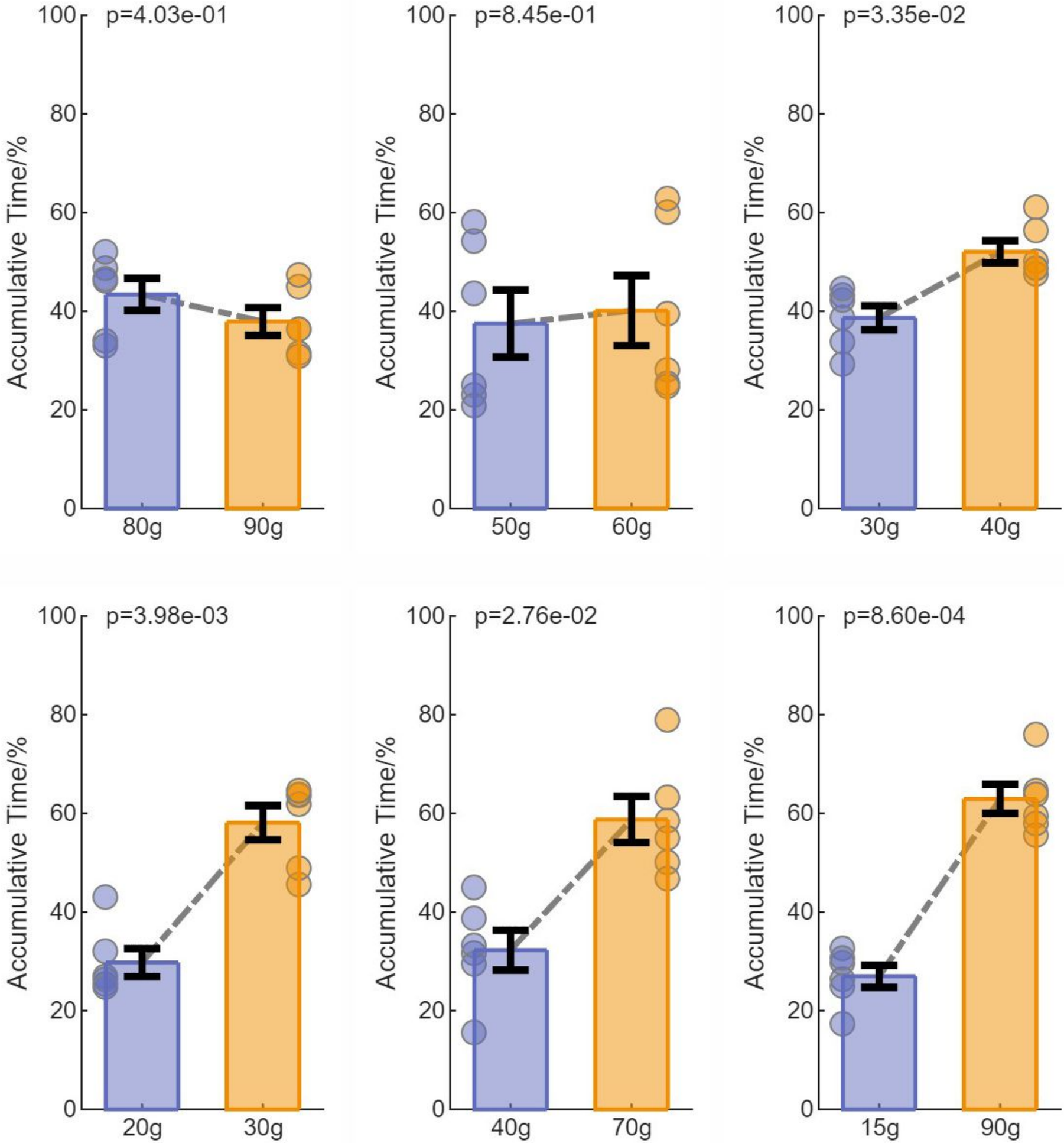
p=4.03e-01
Accumulative Time/%
80g
90g
p=8.45e-01
Accumulative Time/%
50g
60g
p=3.35e-02
Accumulative Time/%
30g
40g
p=3.98e-03
Accumulative Time/%
20g
30g
p=2.76e-02
Accumulative Time/%
40g
70g
p=8.60e-04
Accumulative Time/%
15g
90g
0
20
40
60
80
100

382 **Figure S3. Quantity Discrimination for Additional Food Amounts in Mice, Related to Figure 1**
383 Quantity discrimination behavior for different ratios of food amounts in the C57BL/6J. Paired t-test. Dots
384 manifest individual data. Bars indicate Mean ± SEM.

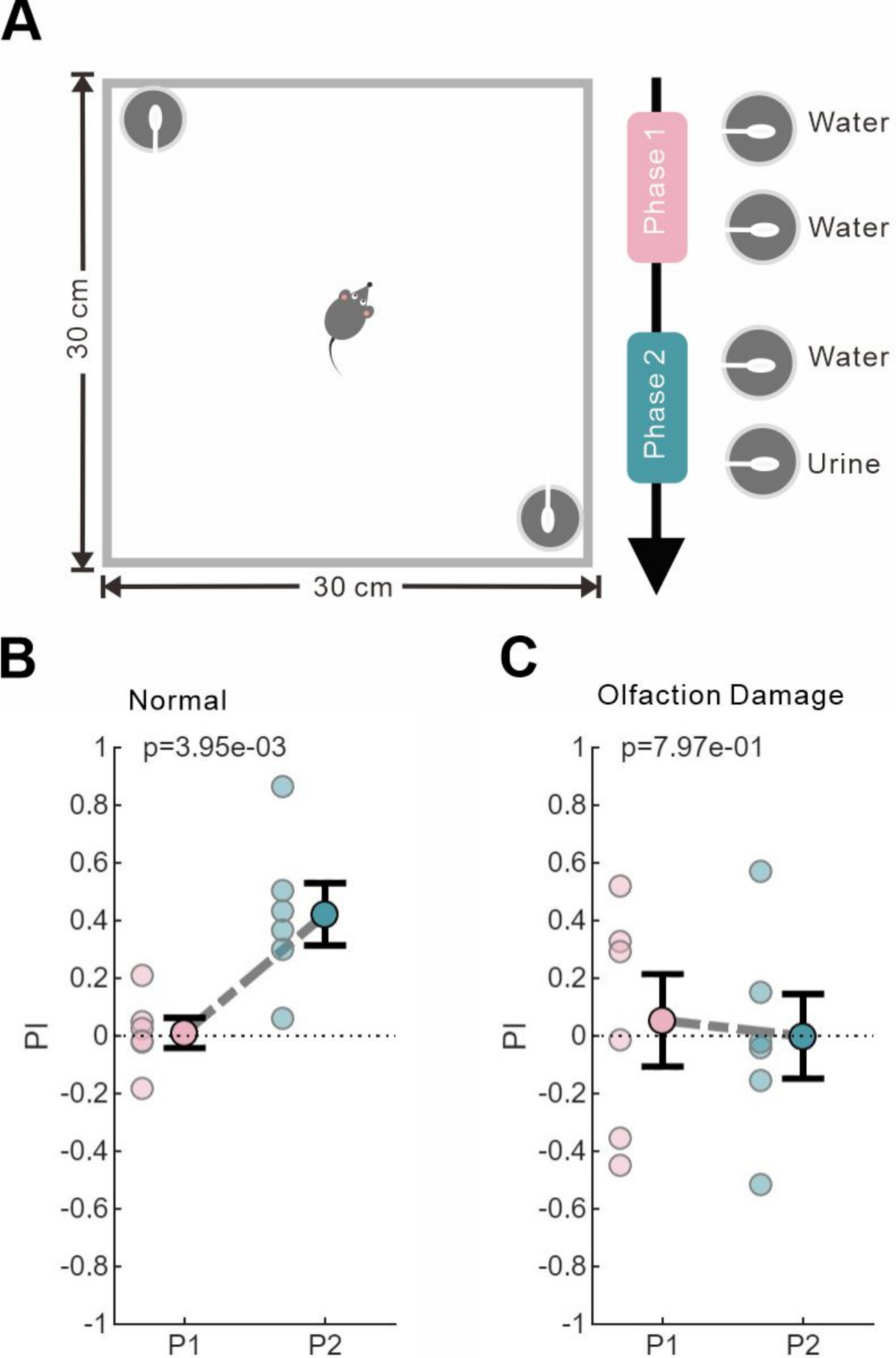
A
30 cm
30 cm
Phase 1
Phase 2
Water
Water
Water
Urine
B
Normal
p=3.95e-03
PI
1
0.8
0.6
0.4
0.2
0
-0.2
-0.4
-0.6
-0.8
-1
P1
P2
C
Olfaction Damage
p=7.97e-01
PI
1
0.8
0.6
0.4
0.2
0
-0.2
-0.4
-0.6
-0.8
-1
P1
P2

Figure S4. Olfactory Test, Related to Figure 1

(A) The exhibition of various olfactory cues in an open arena (STAR Methods).

(B-C) Preference Index (PI) values for olfactory cues during different experimental phases under normal condition (B) or following induced deprivation of olfactory sensation (C).

Paired t-test. Symbols indicate Mean ± SEM. Dots manifest individual data.

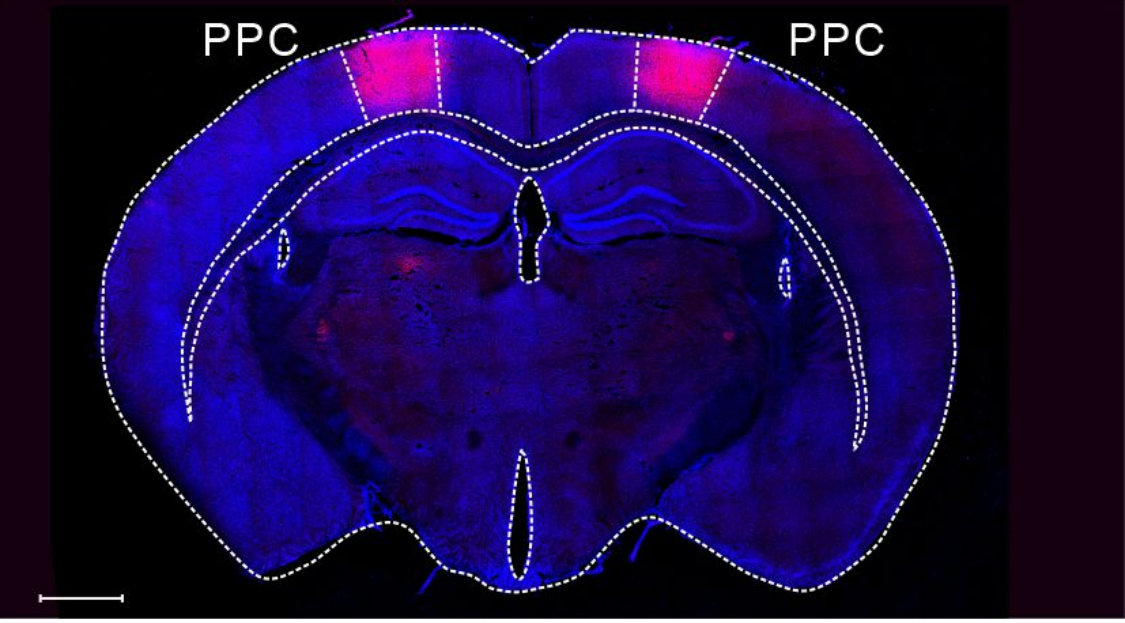
PPC
PPC

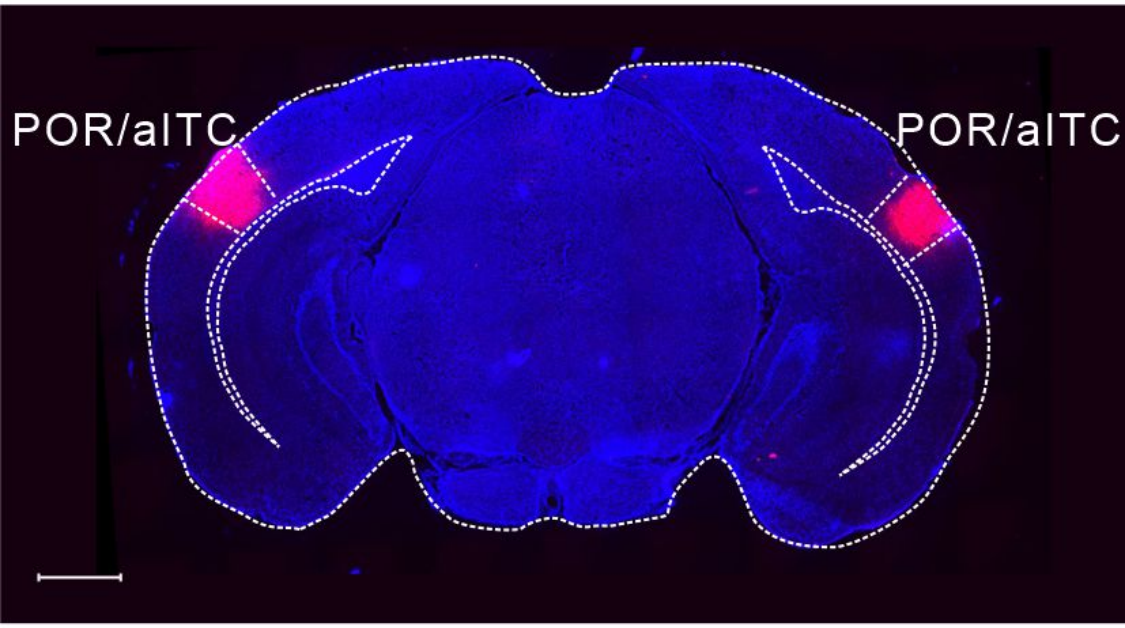
POR/alTC
POR/alTC

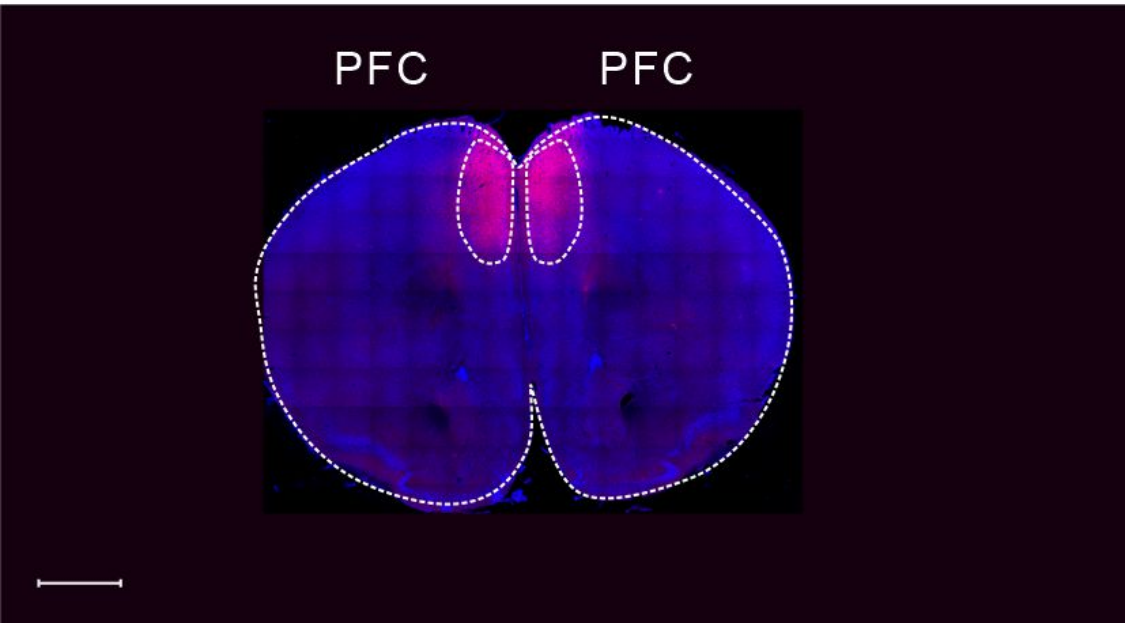
PFC
PFC

Figure S5. Inhibition of Different Cortex Regions, Related to Figure 2

Site-specific delivery of a viral vector expressing an inhibitory channel, pAAV9-hsyn-hM4D(Gi)-mcherry, was performed in different cortex regions: the PPC (top), the POR/aITC (middle), or the PFC (bottom), as described in the Methods. Scale bars: 1mm.

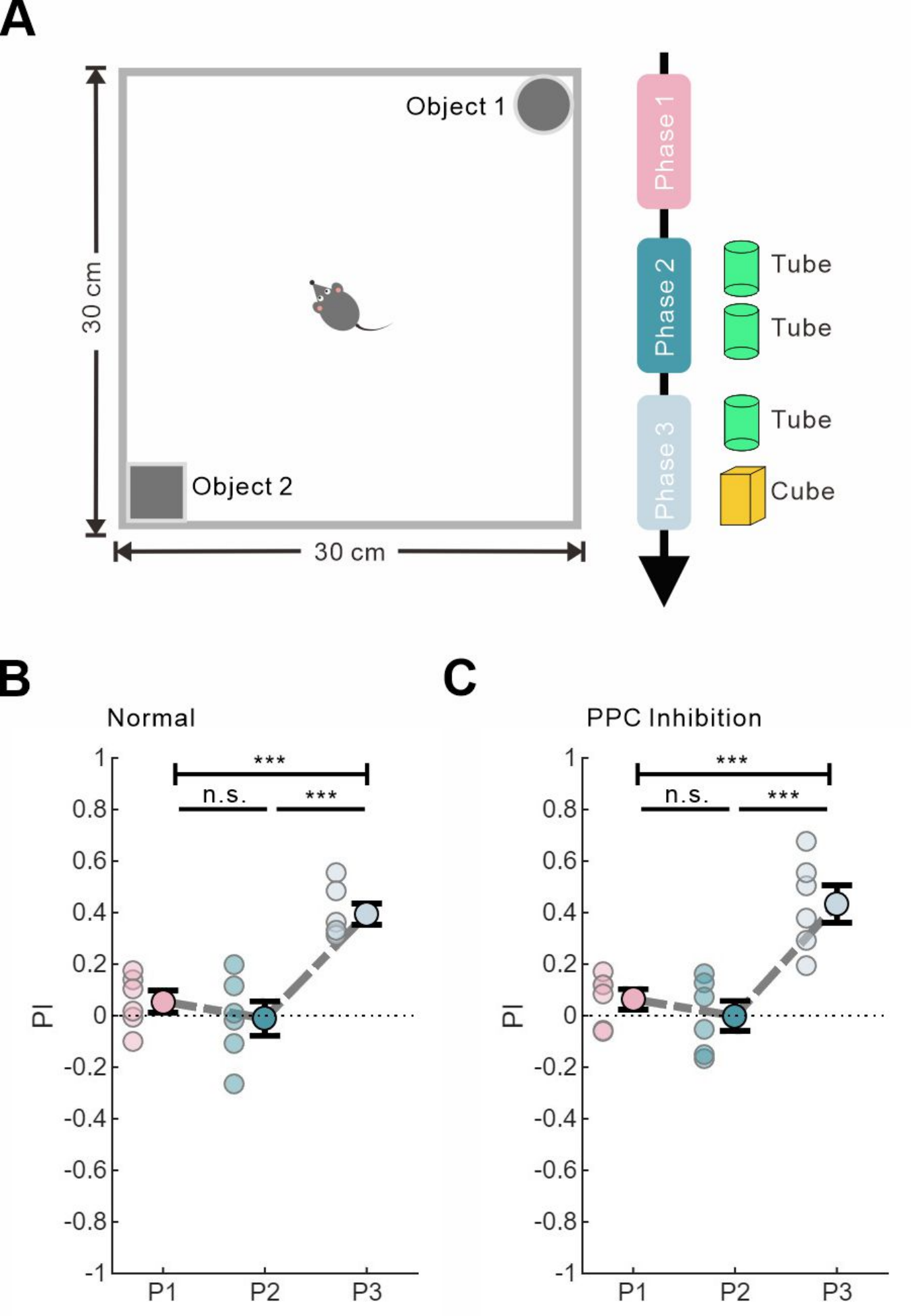
A
Object 1
Object 2
30 cm
30 cm
Phase 1
Phase 2
Phase 3
Tube
Tube
Tube
Cube
B
Normal
C
PPC Inhibition
***
n.s.
***
PI
1
0.8
0.6
0.4
0.2
0
-0.2
-0.4
-0.6
-0.8
-1
P1
P2
P3

Figure S6. Novel Object Recognition Test, Related to Figure 2

(A) The positions of different objects in an open arena (STAR Methods).

(B-C) Preference Index (PI) values for objects during different experimental phases under normal condition (B) or following inhibition of neuronal activities in the PPC (C). One-way ANOVA test, ***$p<0.0005$, **$p<0.005$, (n.s.) $p>0.05$. Symbols indicate Mean ± SEM. Dots manifest individual data.

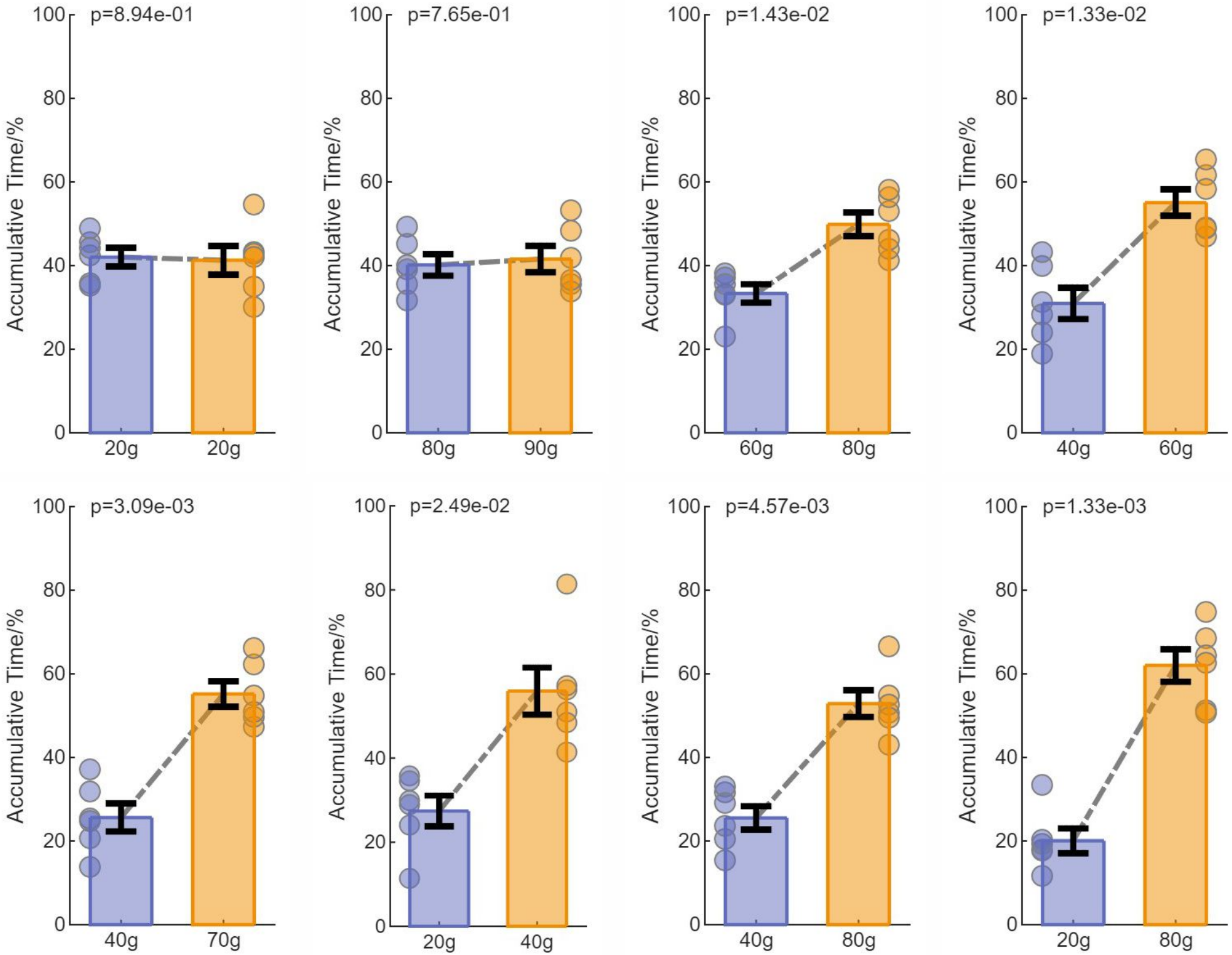
p=8.94e-01
Accumulative Time/%
20g
20g
p=7.65e-01
80g
90g
p=1.43e-02
60g
80g
p=1.33e-02
40g
60g
p=3.09e-03
40g
70g
p=2.49e-02
20g
40g
p=4.57e-03
40g
80g
p=1.33e-03
20g
80g
0
20
40
60
80
100

Figure S7. Quantity Discrimination Behavior During Two-photon Imaging Experiments, Related to Figure 2

(A-H) Quantity discrimination behavior for different amounts of food during the two-photon imaging experiments. Paired t-test. Symbols indicate Mean ± SEM. Dots manifest individual data.

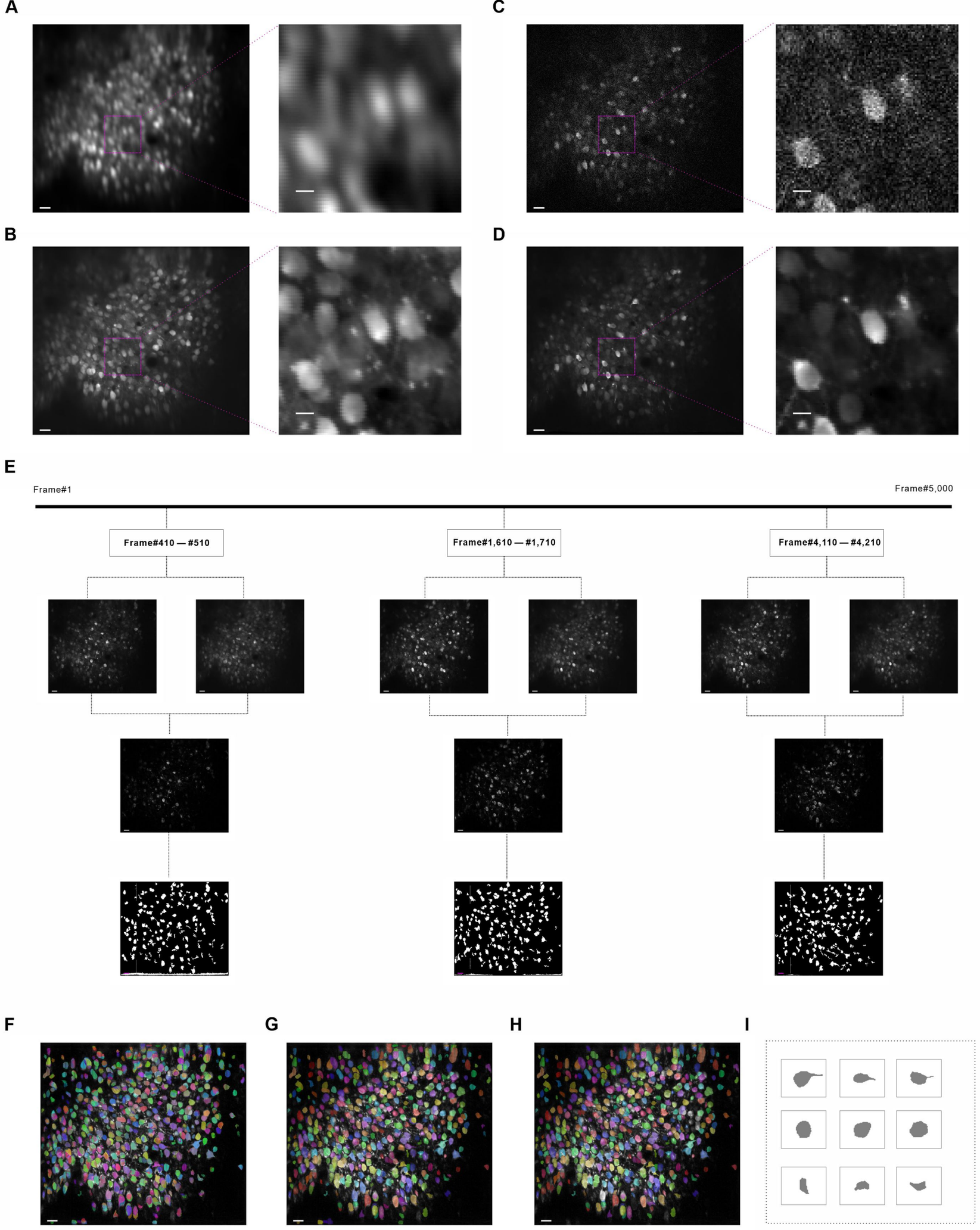
A
C
B
D
E
Frame#1
Frame#5,000
Frame#410 — #510
Frame#1,610 — #1,710
Frame#4,110 — #4,210
F
G
H
I

Figure S8. Two-photon Imaging Data Processing, Related to Figure 2

(A-B) Mean projection images of all frames before (A) and after (B) applying motion correction.

(C-D) A single frame before (C) and after (D) noise reduction.

(E) Three representative periodic blocks, each consisting of 100 consecutive frames. For each block, the maximum projection image (upper left), mean projection image (upper right), max-mean projection image (middle), and corresponding periodic mask (lower) are displayed.

(F-H) Illustrations of the temporal mask (F), spatial mask (G), and soma mask (H).

(I) Examples of typical soma.

Scale bars: 10 pixels (left panels in A-D, E-H) or 30 pixels (right panels in A-D).

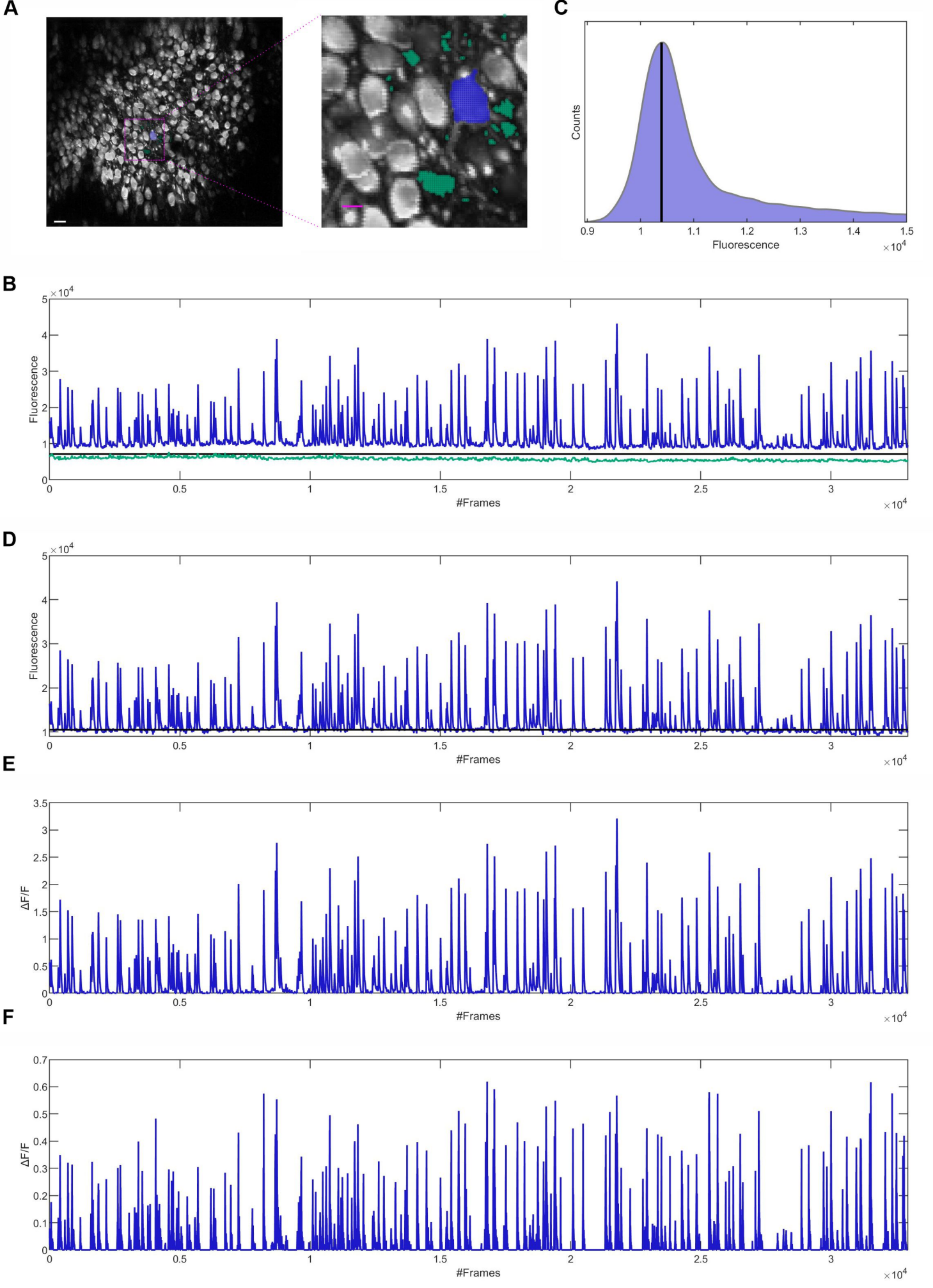
A
C
Counts
Fluorescence
×10^4
B
Fluorescence
#Frames
×10^4
D
Fluorescence
#Frames
×10^4
E
ΔF/F
#Frames
×10^4
F
ΔF/F
#Frames
×10^4

Figure S9. Extraction of Neuronal Activity Signals, Related to Figure 2

(A) A typical neuron (blue) and its corresponding neuropil (green). Scale bars: 10 pixels (left) or 30 pixels (right).

(B) The average fluorescence intensity recorded from the neuron (blue) and its neuropil (green) throughout the entire recording session. The black line indicates the 3-sigma level of the background fluorescence.

(C) Distribution of average fluorescence intensity across individual frames along with the baseline (black line).

(D) The fluorescence trace of the neuron after correction for neuropil contamination and detrending to remove polynomial trends. The black line represents the baseline fluorescence.

(E) The calcium signal of the neuron.

(F) The event signal of the neuron.

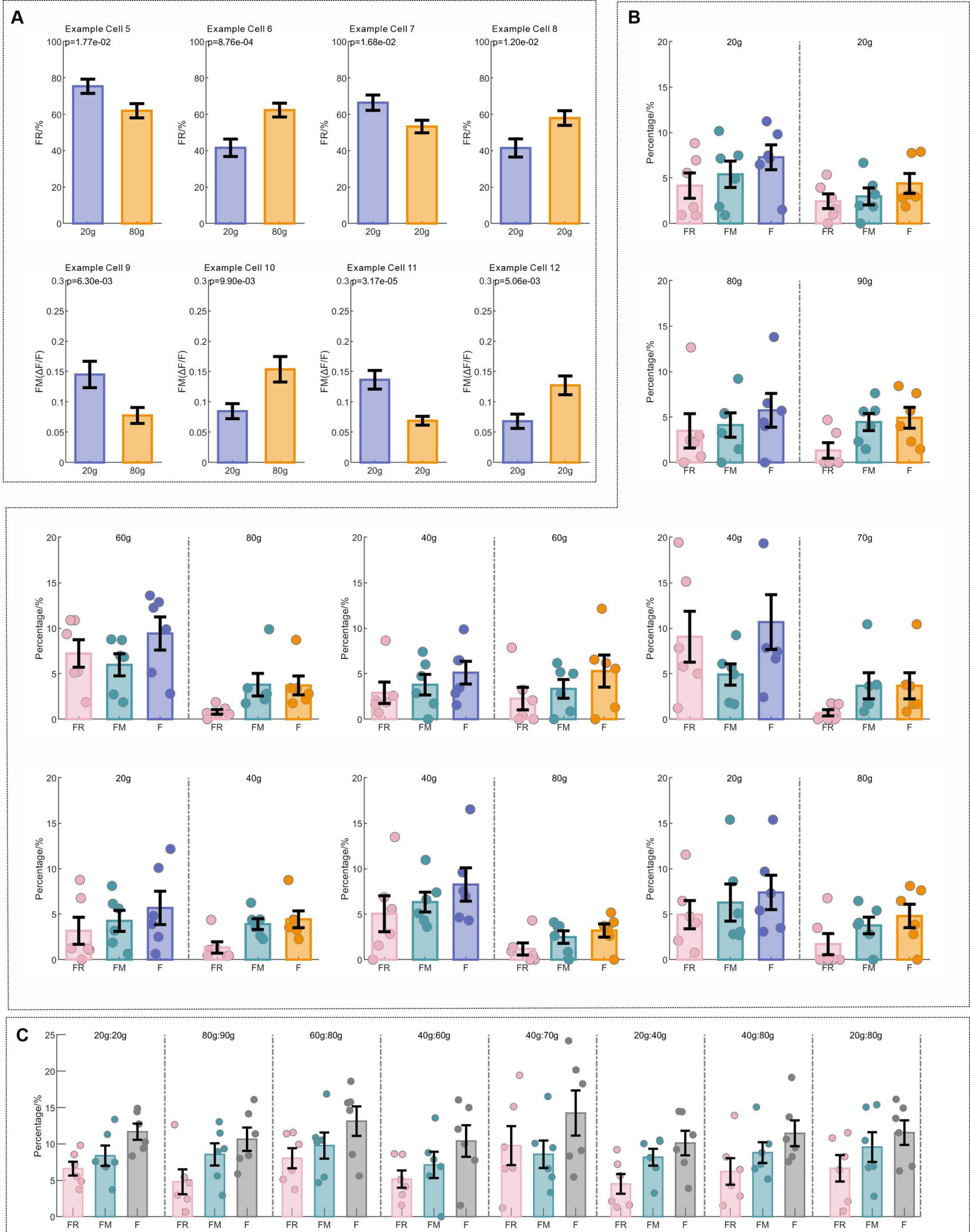
A
Example Cell 5
p=1.77e-02
Example Cell 6
p=8.76e-04
Example Cell 7
p=1.68e-02
Example Cell 8
p=1.20e-02
FR/%
20g
80g
Example Cell 9
p=6.30e-03
Example Cell 10
p=9.90e-03
Example Cell 11
p=3.17e-05
Example Cell 12
p=5.06e-03
FM(ΔF/F)
B
Percentage/%
FR
FM
F
C
20g:20g
80g:90g
60g:80g
40g:60g
40g:70g
20g:40g
40g:80g
20g:80g

Figure S10. Neurons with Preferential Activities at A Given Time, Related to Figure 2

(A) Typical neurons with preferential activities towards a specific amount of food, evaluated by comparing their firing rate (FR, upper panel) or firing magnitude (FM, lower panel) across different foraging zones. Unpaired t-test.

(B) The percentage of neurons showing preferential activities for specific amounts of food, analyzed based on their FR, FM, or overall firing activity, F, which includes both FM and FR.

(C) The overall percentage of neurons with preferential activities in different quantity discrimination assays.

Symbols represent Mean ± SEM, while individual data points are indicated by dots.

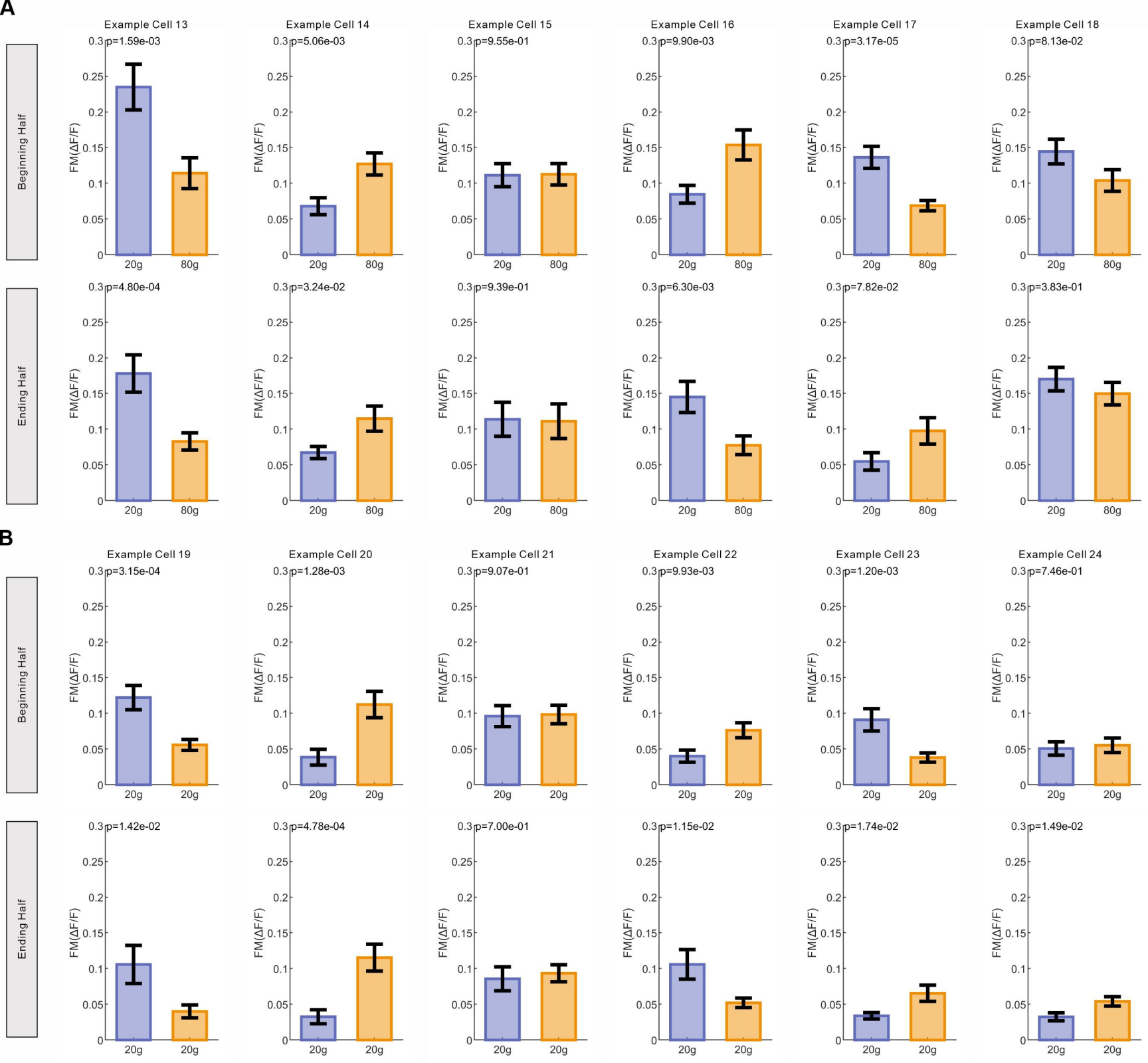
A
Example Cell 13
Example Cell 14
Example Cell 15
Example Cell 16
Example Cell 17
Example Cell 18
Beginning Half
Ending Half
p=1.59e-03
p=5.06e-03
p=9.55e-01
p=9.90e-03
p=3.17e-05
p=8.13e-02
p=4.80e-04
p=3.24e-02
p=9.39e-01
p=6.30e-03
p=7.82e-02
p=3.83e-01
FM(ΔF/F)
20g
80g
B
Example Cell 19
Example Cell 20
Example Cell 21
Example Cell 22
Example Cell 23
Example Cell 24
p=3.15e-04
p=1.28e-03
p=9.07e-01
p=9.93e-03
p=1.20e-03
p=7.46e-01
p=1.42e-02
p=4.78e-04
p=7.00e-01
p=1.15e-02
p=1.74e-02
p=1.49e-02

Figure S11. Preferential Identities of Neurons over Time, Related to Figure 2

(A) Altered preferential activities of six typical neurons in the PPC during the quantity discrimination assay for 20g versus 80g of food at either the beginning (upper) or the ending half (lower).

(B) Preferential activities of six typical neurons in the PPC during the quantity discrimination assay for 20g versus 20g of food at either the beginning (upper) or the ending half (lower).

Unpaired t-test. Symbols indicate Mean ± SEM.

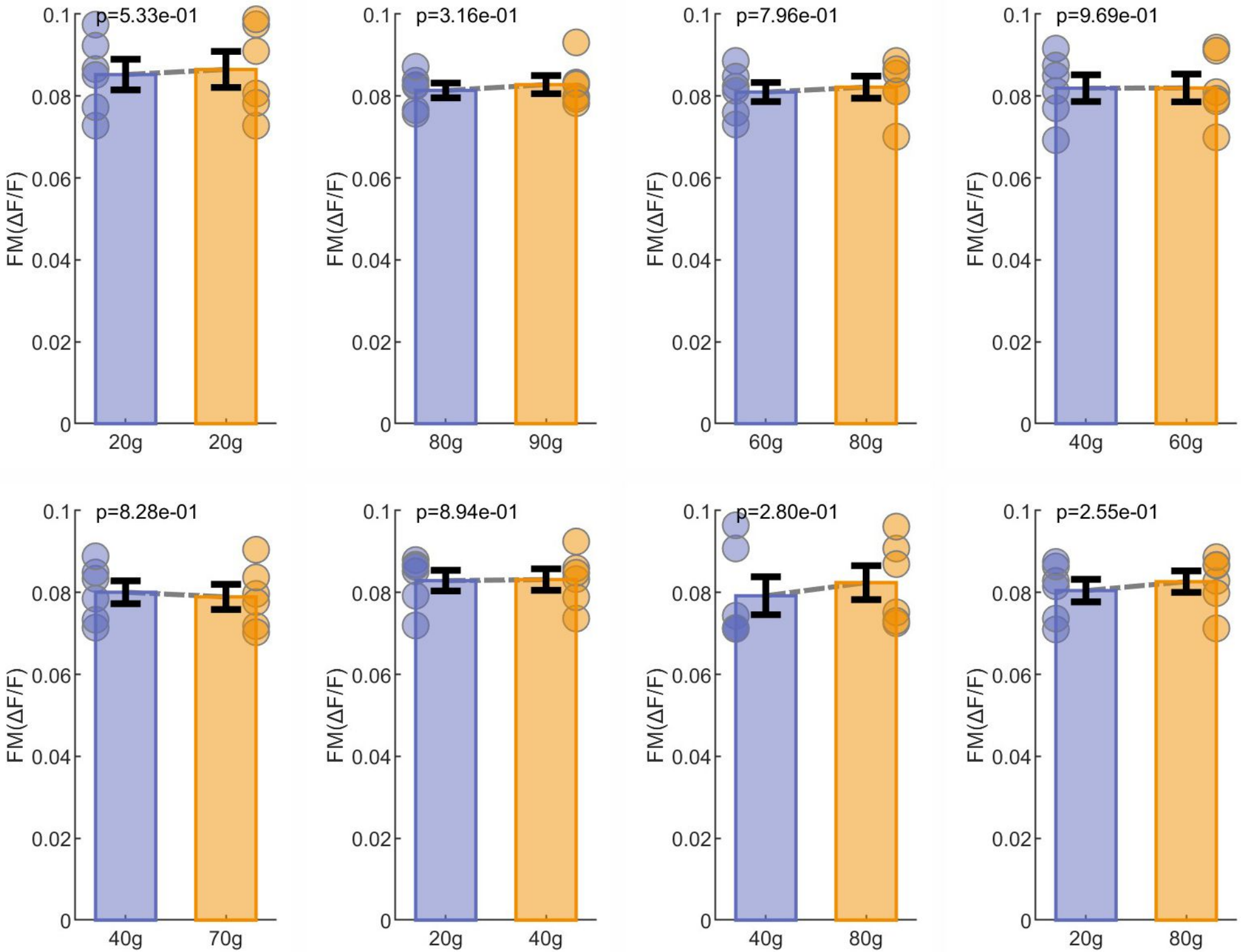
p=5.33e-01
p=3.16e-01
p=7.96e-01
p=9.69e-01
p=8.28e-01
p=8.94e-01
p=2.80e-01
p=2.55e-01
FM(ΔF/F)
0.1
0.08
0.06
0.04
0.02
0
20g
20g
80g
90g
60g
80g
40g
60g
40g
70g
20g
40g
40g
80g
20g
80g

Figure S12. Firing Magnitude of the PPC Neuronal Population, Related to Figure 3

The firing magnitude of the PPC neuronal population when the animals were presented with different amounts of food. Unpaired t-test. Dots manifest individual data. Symbols indicate Mean ± SEM.

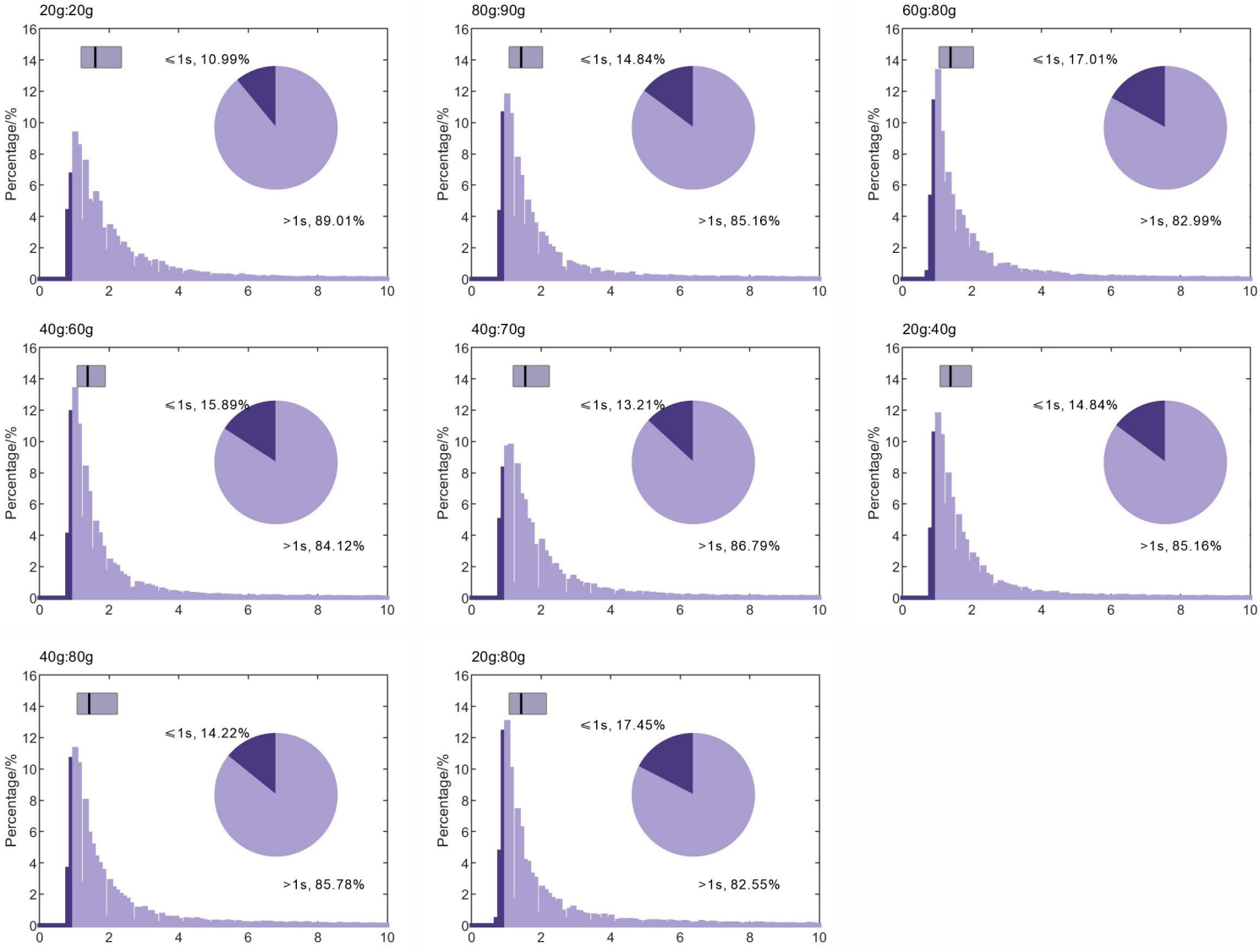
20g:20g
≤1s, 10.99%
>1s, 89.01%
80g:90g
≤1s, 14.84%
>1s, 85.16%
60g:80g
≤1s, 17.01%
>1s, 82.99%
40g:60g
≤1s, 15.89%
>1s, 84.12%
40g:70g
≤1s, 13.21%
>1s, 86.79%
20g:40g
≤1s, 14.84%
>1s, 85.16%
40g:80g
≤1s, 14.22%
>1s, 85.78%
20g:80g
≤1s, 17.45%
>1s, 82.55%
Percentage/%

Figure S13. Duration of Synchronous Firing, Related to Figure 3

The duration of synchronous firing in the PPC neuronal population, illustrated with a pie chart depicting the proportion of patterns classified using a 1-second threshold.

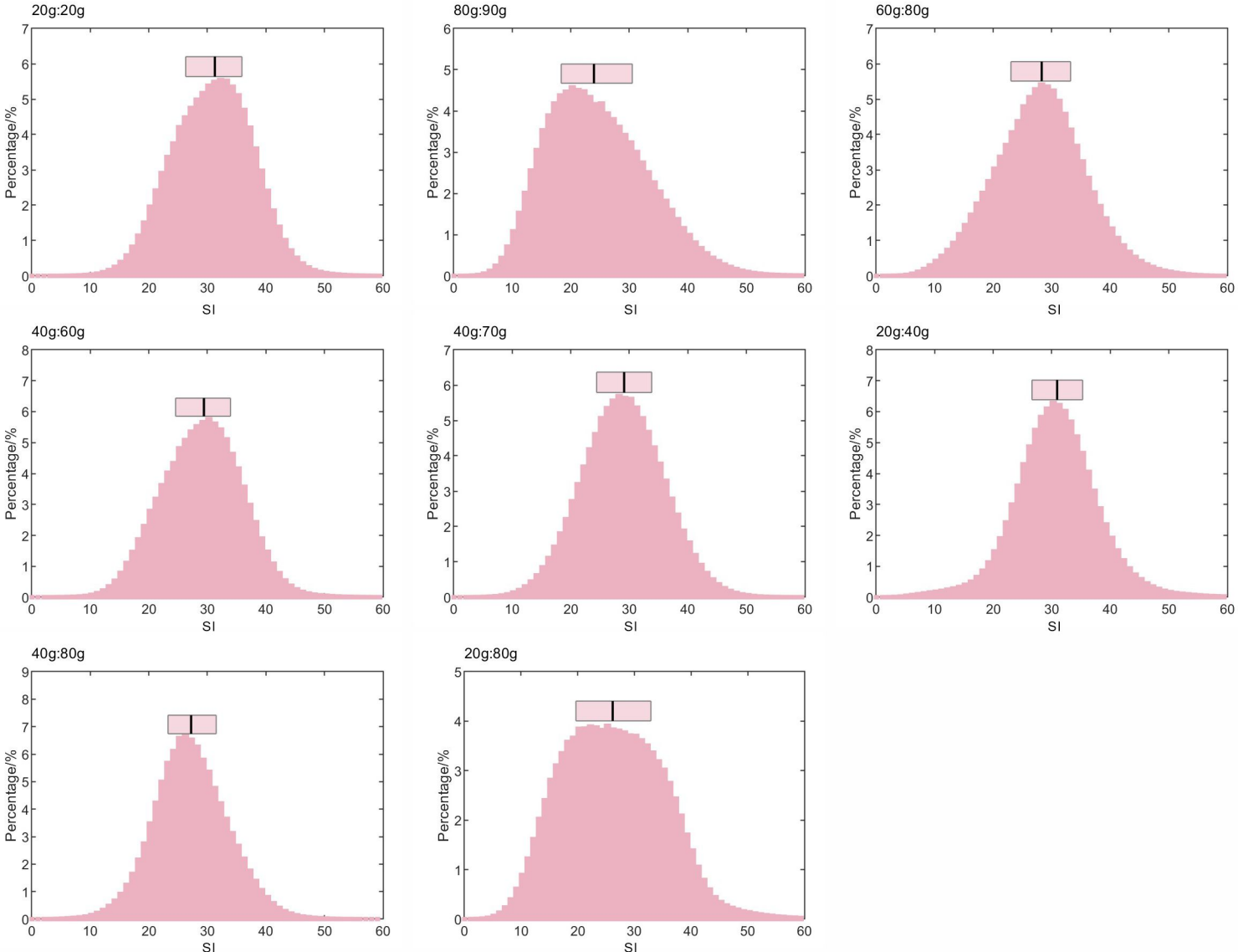
20g:20g
80g:90g
60g:80g
40g:60g
40g:70g
20g:40g
40g:80g
20g:80g
Percentage/%
SI

Figure S14. Distribution of Similarity Index, Related to Figure 3

The distribution of similarity index (SI) between any pair of synchronous firings (STAR Methods).

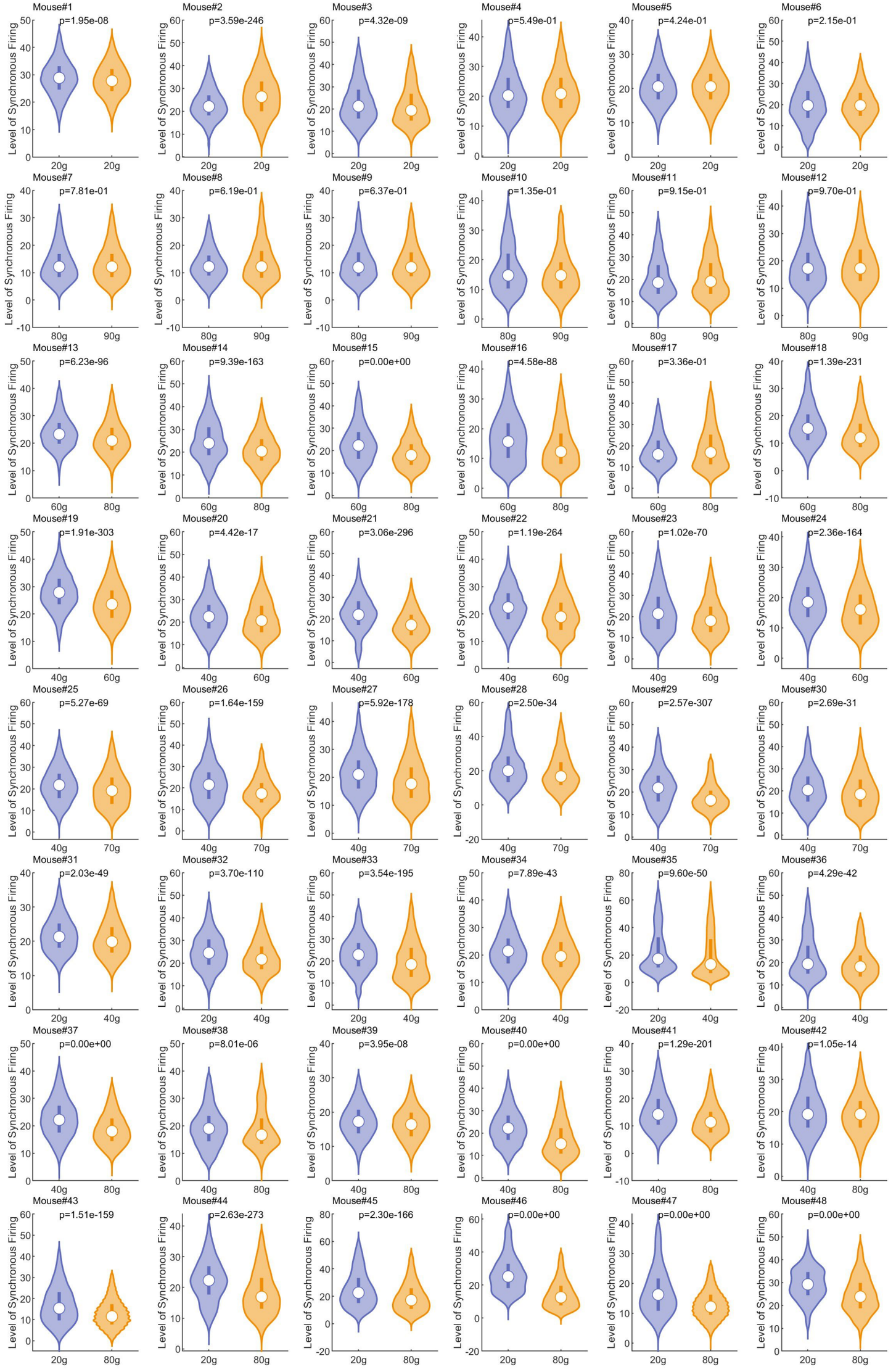
Mouse#1
p=1.95e-08
20g
20g
Mouse#2
p=3.59e-246
20g
20g
Mouse#3
p=4.32e-09
20g
20g
Mouse#4
p=5.49e-01
20g
20g
Mouse#5
p=4.24e-01
20g
20g
Mouse#6
p=2.15e-01
20g
20g
Mouse#7
p=7.81e-01
80g
90g
Mouse#8
p=6.19e-01
80g
90g
Mouse#9
p=6.37e-01
80g
90g
Mouse#10
p=1.35e-01
80g
90g
Mouse#11
p=9.15e-01
80g
90g
Mouse#12
p=9.70e-01
80g
90g
Mouse#13
p=6.23e-96
60g
80g
Mouse#14
p=9.39e-163
60g
80g
Mouse#15
p=0.00e+00
60g
80g
Mouse#16
p=4.58e-88
60g
80g
Mouse#17
p=3.36e-01
60g
80g
Mouse#18
p=1.39e-231
60g
80g
Mouse#19
p=1.91e-303
40g
60g
Mouse#20
p=4.42e-17
40g
60g
Mouse#21
p=3.06e-296
40g
60g
Mouse#22
p=1.19e-264
40g
60g
Mouse#23
p=1.02e-70
40g
60g
Mouse#24
p=2.36e-164
40g
60g
Mouse#25
p=5.27e-69
40g
70g
Mouse#26
p=1.64e-159
40g
70g
Mouse#27
p=5.92e-178
40g
70g
Mouse#28
p=2.50e-34
40g
70g
Mouse#29
p=2.57e-307
40g
70g
Mouse#30
p=2.69e-31
40g
70g
Mouse#31
p=2.03e-49
20g
40g
Mouse#32
p=3.70e-110
20g
40g
Mouse#33
p=3.54e-195
20g
40g
Mouse#34
p=7.89e-43
20g
40g
Mouse#35
p=9.60e-50
20g
40g
Mouse#36
p=4.29e-42
20g
40g
Mouse#37
p=0.00e+00
40g
80g
Mouse#38
p=8.01e-06
40g
80g
Mouse#39
p=3.95e-08
40g
80g
Mouse#40
p=0.00e+00
40g
80g
Mouse#41
p=1.29e-201
40g
80g
Mouse#42
p=1.05e-14
40g
80g
Mouse#43
p=1.51e-159
20g
80g
Mouse#44
p=2.63e-273
20g
80g
Mouse#45
p=2.30e-166
20g
80g
Mouse#46
p=0.00e+00
20g
80g
Mouse#47
p=0.00e+00
20g
80g
Mouse#48
p=0.00e+00
20g
80g
Level of Synchronous Firing

Figure S15. The Levels of Synchronous Firing, Related to Table 1 and Figure 3

The levels of synchronous firing in the PPC neuronal population when individual mice were presented with different food amounts. Mann-Whitney U test.

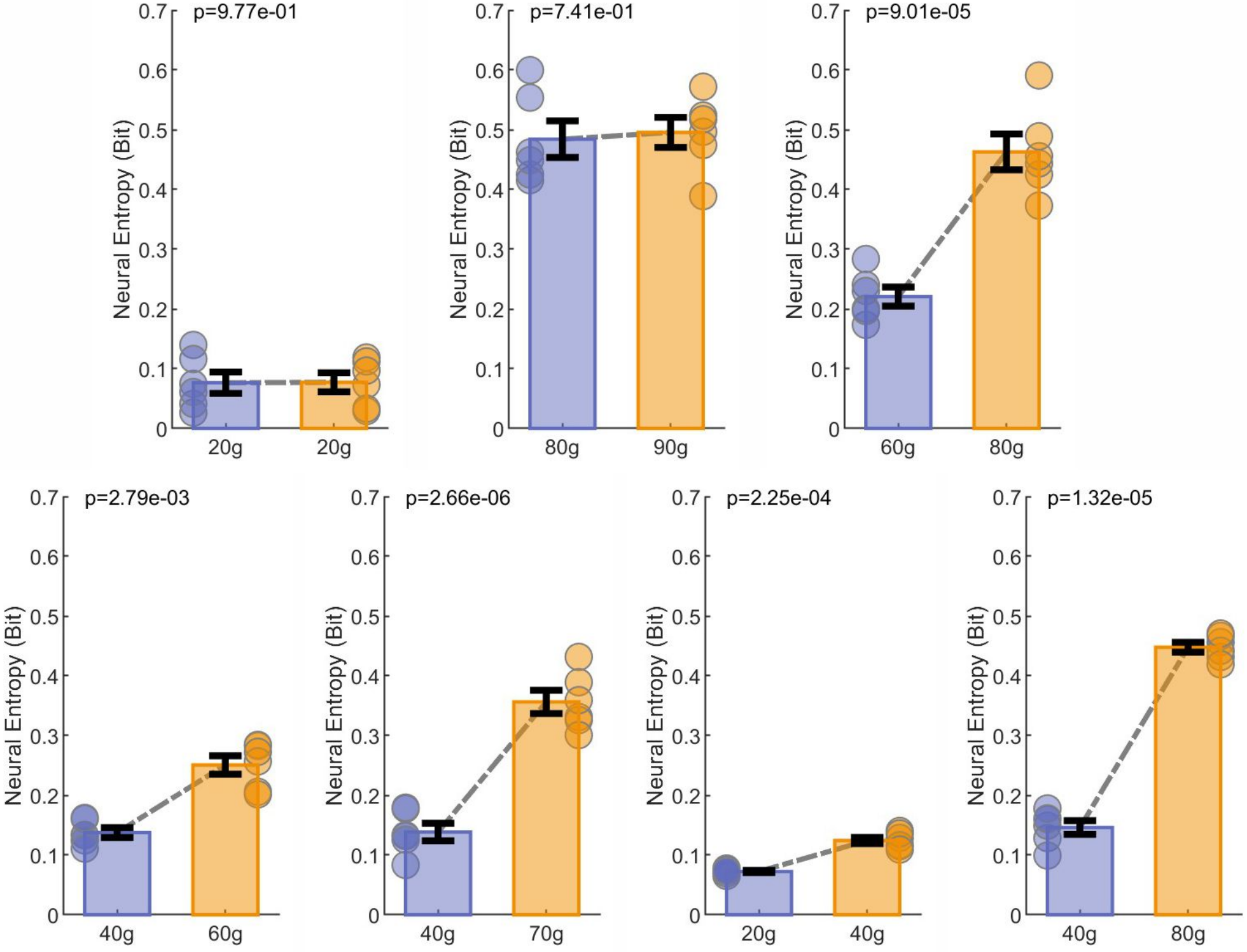
p=9.77e-01
Neural Entropy (Bit)
0.7
0.6
0.5
0.4
0.3
0.2
0.1
0
20g
20g
p=7.41e-01
Neural Entropy (Bit)
80g
90g
p=9.01e-05
Neural Entropy (Bit)
60g
80g
p=2.79e-03
Neural Entropy (Bit)
40g
60g
p=2.66e-06
Neural Entropy (Bit)
40g
70g
p=2.25e-04
Neural Entropy (Bit)
20g
40g
p=1.32e-05
Neural Entropy (Bit)
40g
80g

Figure S16. Neural Entropy Values, Related to Figure 4

The neural entropy values associated with different amounts of food. Paired t-test. Bars represent Mean ± SEM. Dots represent individual data points.

REFERENCES

Abramson, J.Z., Hernández-Lloreda, V., Call, J., and Colmenares, F. (2011). Relative quantity judgments in South American sea lions (Otaria flavescens). Anim Cogn *14*, 695-706.

Addessi, E., Crescimbene, L., and Visalberghi, E. (2008). Food and token quantity discrimination in capuchin monkeys (Cebus apella). Animal cognition *11*, 275-282.

Agrillo, C., Dadda, M., Serena, G., and Bisazza, A. (2008). Do fish count? Spontaneous discrimination of quantity in female mosquitofish. Animal cognition *11*, 495-503.

Alamu, F., Aworinde, H., and Isharufe, W. (2013). A Comparative Study of Ifa Divination and Computer Science. INTERNATIONAL JOURNAL OF INNOVATIVE TECHNOLOGY AND RESEARCH *Volume No. 1*, 524-528.

Ansari, D., Garcia, N., Lucas, E., Hamon, K., and Dhital, B. (2005). Neural correlates of symbolic number processing in children and adults. NeuroReport *16*.

Antunes, M., and Biala, G. (2012). The novel object recognition memory: neurobiology, test procedure, and its modifications. Cognitive Processing *13*, 93-110.

Ashwood, Z.C., Roy, N.A., Stone, I.R., Urai, A.E., Churchland, A.K., Pouget, A., Pillow, J.W., and The International Brain, L. (2022). Mice alternate between discrete strategies during perceptual decision-making. Nature Neuroscience *25*, 201-212.

Balestrieri, A., Gazzola, A., Pellitteri-Rosa, D., and Vallortigara, G. (2019). Discrimination of group numerousness under predation risk in anuran tadpoles. Animal cognition *22*, 223-230.

Beran, M.J. (2001). Summation and numerousness judgments of sequentially presented sets of items by chimpanzees (Pan troglodytes). Journal of comparative psychology (Washington, DC : 1983) *115*, 181-191.

Cantlon, J.F., Brannon, E.M., Carter, E.J., and Pelphrey, K.A. (2006). Functional imaging of numerical processing in adults and 4-y-old children. PLoS biology *4*, e125.

Carandini, M., and Churchland, A.K. (2013). Probing perceptual decisions in rodents. Nature Neuroscience *16*, 824-831.

Castelli, F., Glaser, D.E., and Butterworth, B. (2006). Discrete and analogue quantity processing in the parietal lobe: A functional MRI study. Proceedings of the National Academy of Sciences *103*, 4693-4698.

Chacha, J., Szenczi, P., González, D., Martínez-Byer, S., Hudson, R., and Bánszegi, O. (2020). Revisiting more or less: influence of numerosity and size on potential prey choice in the domestic cat. Animal cognition *23*, 491-501.

Chochon, F., Cohen, L., Van de Moortele, P.-F., and Dehaene, S. (1999). Differential Contributions of the Left and Right Inferior Parietal Lobules to Number Processing. Journal of cognitive neuroscience *11*, 617-630.

Davis, N., Cannistraci, C.J., Rogers, B.P., Gatenby, J.C., Fuchs, L.S., Anderson, A.W., and Gore, J.C. (2009). The neural correlates of calculation ability in children: an fMRI study. Magnetic resonance imaging *27*, 1187-1197.

de Vries, S.E.J., Lecoq, J.A., Buice, M.A., Groblewski, P.A., Ocker, G.K., Oliver, M., Feng, D., Cain, N., Ledochowitsch, P., Millman, D*., et al.* (2020). A large-scale standardized physiological survey reveals functional organization of the mouse visual cortex. Nature Neuroscience *23*, 138-151.

Dehaene, S., Dehaene-Lambertz, G., and Cohen, L. (1998). Abstract representations of numbers in the animal and human brain. Trends in neurosciences *21*, 355-361.

Dehaene, S., Tzourio, N., Frak, V., Raynaud, L., Cohen, L., Mehler, J., and Mazoyer, B. (1996). Cerebral activations during number multiplication and comparison: a PET study. Neuropsychologia *34*, 1097-1106.

Dombeck, D.A., Khabbaz, A.N., Collman, F., Adelman, T.L., and Tank, D.W. (2007). Imaging large-scale neural activity with cellular resolution in awake, mobile mice. Neuron *56*, 43-57.

Driscoll, L.N., Pettit, N.L., Minderer, M., Chettih, S.N., and Harvey, C.D. (2017). Dynamic Reorganization of Neuronal Activity Patterns in Parietal Cortex. Cell *170*, 986-999.e916.

Eger, E., Sterzer, P., Russ, M.O., Giraud, A.L., and Kleinschmidt, A. (2003). A supramodal number representation in human intraparietal cortex. Neuron *37*, 719-725.

Fechner, G. (1860). Elements of psychophysics (Harvard Book List (edited).

Fechner, G.T. (1948). Elements of psychophysics, 1860. In Readings in the history of psychology (East Norwalk, CT, US: Appleton-Century-Crofts), pp. 206-213.

Feigenson, L., Carey, S., and Hauser, M. (2002). The Representations Underlying Infants' Choice of More: Object Files Versus Analog Magnitudes. Psychological Science *13*, 150-156.

Giovannucci, A., Friedrich, J., Gunn, P., Kalfon, J., Brown, B.L., Koay, S.A., Taxidis, J., Najafi, F., Gauthier, J.L., Zhou, P.*, et al.* (2019). CaImAn an open source tool for scalable calcium imaging data analysis. eLife *8*, e38173.

Goard, M.J., Pho, G.N., Woodson, J., and Sur, M. (2016). Distinct roles of visual, parietal, and frontal motor cortices in memory-guided sensorimotor decisions. eLife *5*, e13764.

Gómez-Laplaza, L.M., and Gerlai, R.J.A.C. (2010). Can angelfish (Pterophyllum scalare) count? Discrimination between different shoal sizes follows Weber's law. Animal Cognition *14*, 1-9.

Green, J., Bruno, C.A., Traunmüller, L., Ding, J., Hrvatin, S., Wilson, D.E., Khodadad, T., Samuels, J., Greenberg, M.E., and Harvey, C.D. (2023). A cell-type-specific error-correction signal in the posterior parietal cortex. Nature *620*, 366-373.

Gromley, A., Churchman, M.L., Zindy, F., and Sherr, C.J. (2009). Transient expression of the Arf tumor suppressor during male germ cell and eye development in Arf-Cre reporter mice. Proceedings of the National Academy of Sciences of the United States of America *106*, 6285-6290.

Halberda, J., and Feigenson, L. (2008). Developmental change in the acuity of the "Number Sense": The Approximate Number System in 3-, 4-, 5-, and 6-year-olds and adults. Developmental psychology *44*, 1457-1465.

Hanks, T.D., and Summerfield, C. (2017). Perceptual Decision Making in Rodents, Monkeys, and Humans. Neuron *93*, 15-31.

Harvey, C.D., Coen, P., and Tank, D.W. (2012). Choice-specific sequences in parietal cortex during a virtual-navigation decision task. Nature *484*, 62-68.

Hopfield, J.J. (1982). Neural networks and physical systems with emergent collective computational abilities. Proceedings of the National Academy of Sciences of the United States of America *79*, 2554-2558.

Hwang, E.J., Dahlen, J.E., Mukundan, M., and Komiyama, T. (2017). History-based action selection bias in posterior parietal cortex. Nature Communications *8*, 1242.

Jaccard, P. (1901). Etude comparative de la distribution florale dans une portion des Alpes et des Jura. ulletin del la Société Vaudoise des Sciences Naturelles.

Kalesnykas, G., Oglesby, E.N., Zack, D.J., Cone, F.E., Steinhart, M.R., Tian, J., Pease, M.E., and Quigley, H.A. (2012). Retinal ganglion cell morphology after optic nerve crush and experimental glaucoma. Investigative ophthalmology & visual science *53*, 3847-3857.

Kaszas, A., Szalay, G., Slézia, A., Bojdán, A., Vanzetta, I., Hangya, B., Rózsa, B., O'Connor, R., and Moreau, D. (2021). Two-photon GCaMP6f imaging of infrared neural stimulation evoked calcium signals in mouse cortical neurons in vivo. Scientific Reports *11*, 9775.

Kaufmann, L., Vogel, S.E., Wood, G., Kremser, C., Schocke, M., Zimmerhackl, L.-B., and Koten, J.W. (2008). A developmental fMRI study of nonsymbolic numerical and spatial processing. Cortex *44*, 376-385.

Keiser, M.S., Chen, Y.H., and Davidson, B.L. (2018). Techniques for Intracranial Stereotaxic Injections of Adeno-Associated Viral Vectors in Adult Mice. Current protocols in mouse biology *8*, e57.

Kerr, J.N.D., Greenberg, D., and Helmchen, F. (2005). Imaging input and output of neocortical networks in vivo. Proceedings of the National Academy of Sciences *102*, 14063-14068.
Khatiwada, S., and Burmeister, S.S. (2022). Quantity discrimination in a spontaneous task in a poison frog. Animal cognition *25*, 27-32.
Komiyama, T., Sato, T.R., O'Connor, D.H., Zhang, Y.-X., Huber, D., Hooks, B.M., Gabitto, M., and Svoboda, K. (2010). Learning-related fine-scale specificity imaged in motor cortex circuits of behaving mice. Nature *464*, 1182-1186.
Krusche, P., Uller, C., and Dicke, U. (2010). Quantity discrimination in salamanders. Journal of Experimental Biology *213*, 1822-1828.
Kuan, A.T., Bondanelli, G., Driscoll, L.N., Han, J., Kim, M., Hildebrand, D.G.C., Graham, B.J., Wilson, D.E., Thomas, L.A., Panzeri, S.*, et al.* (2024). Synaptic wiring motifs in posterior parietal cortex support decision-making. Nature *627*, 367-373.
LaChance, P.A., Todd, T.P., and Taube, J.S. (2019). A sense of space in postrhinal cortex. Science (New York, NY) *365*, eaax4192.
Le Merre, P., Ährlund-Richter, S., and Carlén, M. (2021). The mouse prefrontal cortex: Unity in diversity. Neuron *109*, 1925-1944.
Lecoq, J., Oliver, M., Siegle, J.H., Orlova, N., Ledochowitsch, P., and Koch, C. (2021). Removing independent noise in systems neuroscience data using DeepInterpolation. Nature Methods *18*, 1401-1408.
Lee, J.J., Krumin, M., Harris, K.D., and Carandini, M. (2022). Task specificity in mouse parietal cortex. Neuron *110*, 2961-2969.e2965.
Lewis, K.P., Jaffe, S., and Brannon, E.M. (2005). Analog number representations in mongoose lemurs (Eulemur mongoz): evidence from a search task. Anim Cogn *8*, 247-252.
Lucon-Xiccato, T., Dadda, M., Gatto, E., and Bisazza, A. (2017). Development and testing of a rapid method for measuring shoal size discrimination. Animal cognition *20*, 149-157.
Lyamzin, D., and Benucci, A. (2019). The mouse posterior parietal cortex: Anatomy and functions. Neurosci Res *140*, 14-22.
Mathis, A., Mamidanna, P., Cury, K.M., Abe, T., Murthy, V.N., Mathis, M.W., and Bethge, M. (2018). DeepLabCut: markerless pose estimation of user-defined body parts with deep learning. Nature Neuroscience *21*, 1281-1289.
McBride, K., Slotnick, B., and Margolis, F.L. (2003). Does intranasal application of zinc sulfate produce anosmia in the mouse? An olfactometric and anatomical study. Chemical senses *28*, 659-670.
Miletto Petrazzini, M.E., and Wynne, C.D. (2016). What counts for dogs (Canis lupus familiaris) in a quantity discrimination task? Behavioural processes *122*, 90-97.
Minderer, M., Brown, K.D., and Harvey, C.D. (2019). The Spatial Structure of Neural Encoding in Mouse Posterior Cortex during Navigation. Neuron *102*, 232-248.e211.
Morcos, A.S., and Harvey, C.D. (2016). History-dependent variability in population dynamics during evidence accumulation in cortex. Nature Neuroscience *19*, 1672-1681.
Nieder, A. (2016). The neuronal code for number. Nature Reviews Neuroscience *17*, 366-382.
Nieder, A., Diester, I., and Tudusciuc, O. (2006). Temporal and spatial enumeration processes in the primate parietal cortex. Science *313*, 1431-1435.
Nieder, A., Freedman, D.J., and Miller, E.K. (2002). Representation of the quantity of visual items in the primate prefrontal cortex. Science (New York, NY) *297*, 1708-1711.
Nieder, A., and Miller, E.K. (2003). Coding of Cognitive Magnitude: Compressed Scaling of Numerical Information in the Primate Prefrontal Cortex. Neuron *37*, 149-157.
Nieder, A., and Miller, E.K. (2004). A parieto-frontal network for visual numerical information in the monkey. Proceedings of the National Academy of Sciences *101*, 7457-7462.

Orlandi, J.G., Abdolrahmani, M., Aoki, R., Lyamzin, D.R., and Benucci, A. (2023). Distributed context-dependent choice information in mouse posterior cortex. Nature Communications *14*, 192.
Petersen, C.C.H. (2019). Sensorimotor processing in the rodent barrel cortex. Nature Reviews Neuroscience *20*, 533-546.
Pho, G.N., Goard, M.J., Woodson, J., Crawford, B., and Sur, M. (2018). Task-dependent representations of stimulus and choice in mouse parietal cortex. Nature Communications *9*, 2596.
Piazza, M., Mechelli, A., Price, C.J., and Butterworth, B. (2006). Exact and approximate judgements of visual and auditory numerosity: An fMRI study. Brain Research *1106*, 177-188.
Piffer, L., Agrillo, C., and Hyde, D.C. (2012). Small and large number discrimination in guppies. Animal cognition *15*, 215-221.
Pinel, P., Dehaene, S., Rivière, D., and LeBihan, D. (2001). Modulation of parietal activation by semantic distance in a number comparison task. NeuroImage *14*, 1013-1026.
Pinskiy, V., Tolpygo, A.S., Jones, J., Weber, K., Franciotti, N., and Mitra, P.P. (2013). A low-cost technique to cryo-protect and freeze rodent brains, precisely aligned to stereotaxic coordinates for whole-brain cryosectioning. J Neurosci Methods *218*, 206-213.
Pittler, S.J., and Baehr, W. (1991). Identification of a nonsense mutation in the rod photoreceptor cGMP phosphodiesterase beta-subunit gene of the rd mouse. Proceedings of the National Academy of Sciences of the United States of America *88*, 8322-8326.
Pnevmatikakis, E.A., and Giovannucci, A. (2017). NoRMCorre: An online algorithm for piecewise rigid motion correction of calcium imaging data. Journal of Neuroscience Methods *291*, 83-94.
Posner, M.I., Weible, A.P., Voelker, P., Rothbart, M.K., and Niell, C.M. (2022). Decision Making as a Learned Skill in Mice and Humans. Frontiers in Neuroscience *Volume 16 - 2022*.
Quian Quiroga, R., and Panzeri, S. (2009). Extracting information from neuronal populations: information theory and decoding approaches. Nature reviews Neuroscience *10*, 173-185.
Sawamura, H., Shima, K., and Tanji, J. (2002). Numerical representation for action in the parietal cortex of the monkey. Nature *415*, 918-922.
Schaffer, A., Caicoya, A.L., Widdig, A., Holland, R., and Amici, F. (2025). Quantity discrimination in 9 ungulate species: Individuals take item number and size into account to discriminate quantities. Cognition *254*, 105979.
Shannon, C.E. (1948). A mathematical theory of communication. The Bell System Technical Journal *27*, 379-423.
Sheardown, E., Torres-Perez, J.V., Anagianni, S., Fraser, S.E., Vallortigara, G., Butterworth, B., Miletto-Petrazzini, M.E., and Brennan, C.H. (2022). Characterizing ontogeny of quantity discrimination in zebrafish. Proceedings of the Royal Society B: Biological Sciences *289*, 20212544.
Sheng, W., Huang, X., Xie, Y., Tsakiris, M.C., and Yang, Y. (2024). Posterior parietal cortex mediates rarity-induced decision bias and learning under uncertainty. bioRxiv, 2024.2010.2025.620383.
Song, Y.H., Kim, J.H., Jeong, H.W., Choi, I., Jeong, D., Kim, K., and Lee, S.H. (2017). A Neural Circuit for Auditory Dominance over Visual Perception. Neuron *93*, 940-954.e946.
Tsai, M.-Y., Huang, C.-T., Lin, C.-Y., Lee, M.-P., Yang, F.-S., Li, M., Chang, Y.-M., Watanabe, K., Taniguchi, T., Ho, C.-H*., et al.* (2023). A reconfigurable transistor and memory based on a two-dimensional heterostructure and photoinduced trapping. Nature Electronics *6*, 755-764.
VanMarle, K., Aw, J., McCrink, K., and Santos, L.R. (2006). How capuchin monkeys (Cebus apella) quantify objects and substances. J Comp Psychol *120*, 416-426.
Wang, S., Gao, H., Ueoka, Y., Ishizu, K., and Funamizu, A. (2024). Global neural encoding of behavioral strategies in mice during perceptual decision-making task with two different sensory patterns. iScience *27*.
Weber, E. (1834). De pulsu, resorptione, auditu et tactu. Annotationes anatomicae et physiologicae.

639 Welker, E., and Loos, H.V.d. (1986). Quantitative correlation between barrel-field size and the sensory
640 innervation of the whiskerpad: a comparative study in six strains of mice bred for different patterns of
641 mystacial vibrissae. The Journal of Neuroscience *6*, 3355.
642 Yang, D., Yang, X., Peng, J., Lu, J., Hao, X., Guo, S., Li, J., Chen, R., Xu, C., Xiang, L.*, et al.* (2025). Genetic
643 association between posterior parietal cortex and intelligence. bioRxiv, 2025.2003.2021.644693.
644 Yang, T.I., and Chiao, C.C. (2016). Number sense and state-dependent valuation in cuttlefish.
645 Proceedings Biological sciences *283*.
646 Zacharopoulos, G., Sella, F., Emir, U., and Cohen Kadosh, R. (2021). The relation between parietal GABA
647 concentration and numerical skills. Scientific reports *11*, 17656.
648 Zhong, L., Zhang, Y., Duan, C.A., Deng, J., Pan, J., and Xu, N.-l. (2019). Causal contributions of parietal
649 cortex to perceptual decision-making during stimulus categorization. Nature Neuroscience *22*, 963-973.
650 Zong, W., Wu, R., Li, M., Hu, Y., Li, Y., Li, J., Rong, H., Wu, H., Xu, Y., Lu, Y.*, et al.* (2017). Fast high-
651 resolution miniature two-photon microscopy for brain imaging in freely behaving mice. Nat Methods *14*,
652 713-719.
653 Zou, J., Wang, W., Pan, Y.W., Lu, S., and Xia, Z. (2015). Methods to measure olfactory behavior in mice.
654 Current protocols in toxicology *63*, 11.18.11-11.18.21.

655 **STAR★METHODS**

656 **KEY RESOURCES TABLE**

REAGENT/RESOURCE	SOURCE	IDENTIFIER
Experimental Models: Organisms/Strains		
C57BL/6J	Charles River Laboratory	https://www.vitalriver.com
129		
BALB/c		
FVB/NJ		
$Arf^{FL/+}$ (023323)	Jackson Laboratories	https://www.jax.org
Mouse Food		
Lab Mice Diet (1022)	Beijing HFK Bioscience	https://www.hfkbio.com/
Virus Strains		
pAAV9-hsyn-hM4D(Gi)-mcherry	Weizhen Company	https://www.wzbio.com.cn
pAAV-hsyn-gCamp6f-WPRE-hGHpA		
Software and Algorithms		
MATLAB R2020a	MathWorks	https://www.mathworks.com
NoRMCorre	GitHub	https://github.com/flatironinstitute/NoRMCorre
DeepInterpolation		https://github.com/AllenInstitute/deepinterpolation
Two-photon Microscopy		
FHIRM-TPM	Raygene Health Company	https://www.raygenitm.com

657

658 **EXPERIMENTAL MODEL AND STUDY PARTICIPANT DETAILS**

659 All experimental procedures were approved by the laboratory animal resources center at Westlake
660 University. The male mice at age of 6-8 weeks from C57BL/6J, 129, BALB/c, FVB/NJ, and $Arf^{FL/+}$ strains
661 were used for the quantity discrimination assay. Only C57BL/6J mice were used for reverse chemical
662 genetics, two-photon imaging experiments, olfactory test and novel object recognition test. Mice were
663 housed under a reversed 12-hour day/12-hour night cycle at 20℃-26℃ and were restrained from food for
664 48 hours before experiments.

665 **METHOD DETAILS**

666 **The food-based assay**

667 Each mouse was individually placed at the center of an open field arena measuring 30×30×50cm (length ×
668 width × height) for a 10-minute habituation period, as depicted in Figure 1A, to acclimate to the environment.
669 Subsequently, designed amounts of food (Lab Mice Diet) were placed at random at diagonally opposite
670 corners of the arena. The behavior of each mouse was recorded with an overhead camera for 60 minutes.
671 The remaining food in each container was subsequently measured to determine consumption. Recorded
672 videos were analyzed with the DeepLabCut software, which enabled precise tracking of mouse movement
673 (Mathis et al., 2018). Specific anatomical features, including the nose, ears and tail, were annotated for a
674 detailed assessment of behavior. Using a customized MATLAB program, the distance of the mouse's nose
675 to each food container was computed and used to calculate the percentage of time spent in proximity to
676 interpret foraging preferences. In a series of experiments, different food amount ratios were tested using
677 specific combinations, as outlined in Table 1 and S1. In a set of visual deception experiment, 40g and 80g

678 of food ratio 1:2 were used; however, conspicuity was manipulated by concealing a plastic block within the
679 container holding 40g to simulate a similar visual volume as the 80g container.

680 **Evaluation of Weber-Fechner law in the context of quantity discrimination**

681 We designed various food amount ratios (Table S1) and measured the ratios of the accumulated time mice
682 spent in designated foraging zones. To analyze the relationship, we applied two mathematical models
683 including polynomial regression and a sigmoid function. The data were most accurately described by a
684 sigmoid curve (Figure 1F). From the sigmoid curve, we derived the Weber fraction, a metric that quantifies
685 the smallest detectable difference in stimulus intensity perceivable by the subject (Weber, 1834). In this
686 context, it was adapted to measure the discernible differences in food amounts. The inflection point of the
687 curve, occurring at approximately 1.37 (Weber fraction value 0.37), was critical for determining this value.

688 **Sensory input for discriminating different food amounts**

689 Tactile deprivation was induced by carefully trimming the whiskers of the mice 10 minutes prior to testing
690 (Welker and Loos, 1986). Transient anosmia in the mice was induced by administering 100μl of 5% ZnSO4
691 into each naris 24 hours before conducting the assay or olfactory test (McBride et al., 2003). Optic nerve
692 damage was induced by crushing the optic nerve 24 hours before testing (Kalesnykas et al., 2012), and a
693 mutation in the *Pde6b* gene attributed to the early onset retinal degeneration specifically in the FVB/NJ
694 mice (Pittler and Baehr, 1991). Transient expression of Arf in the *Cdkn2a* locus resulted in aberrant
695 postnatal proliferation in the eye and subsequent blindness in the $Arf^{FL/+}$ mice (Gromley et al., 2009).

696 **Olfactory test**

697 The olfactory test for rodents comprises two distinct phases (Zou et al., 2015). During the first phase (P1),
698 containers with swabs soaked in water, which served as nonsocial cues, were placed at opposite corners
699 of the open field arena. Subsequently, in the second phase (P2), one of the water-soaked swabs was
700 replaced with a swab permeated with urine, providing a social olfactory cue (Figure S4). Mice were allowed
701 to explore freely and detect olfactory cues for a period of 10 minutes during both P1 and P2. The movement
702 of individual mice was analyzed similarly to that in the food quantity discrimination assay. To evaluate
703 olfactory preference in the mice, a Preference Index (PI) was calculated by measuring their discrimination
704 between the nonsocial and social olfactory stimuli. The PI is determined by the ratio of the difference to the
705 sum of the accumulative time spent in the zones with social or nonsocial cues. A positive PI value indicated
706 an individual mouse's interest in social cues.

707 **Stereotaxic viral injection, reverse chemical genetics, and two-photon imaging**

708 Mice were positioned on the stereoscopic positioning instrument after deep anesthesia induced by 1.5 to
709 2.5% isoflurane in oxygen (Keiser et al., 2018). The skull's fascia was removed with 4% phosphate-buffered
710 saline following the incision of the mouse scalp. The bregma point served as the coordination origin for
711 identifying the virus injection locations in the POR/aITC (AP: -3.00mm; ML: ±4.3mm: DV: 0.35mm), or the
712 PPC (AP: -2.00mm; ML: ±1.6mm: DV: 0.35mm), or the PFC (AP: 2.43mm; ML: ±0.4mm: DV: 1.20mm)
713 (LaChance et al., 2019; Le Merre et al., 2021; Lyamzin and Benucci, 2019).

714 For experiments involving reverse chemical genetics, a total of 200nl pAAV9-hsyn-hM4D(Gi)-mcherry
715 ($1\times10^{13} GC/ml$) virus was slowly injected at a rate of 50nl/min into the bilateral regions of the specific
716 cortex regions (Keiser et al., 2018). The quantity discrimination behavior or the novel object recognition of
717 individual mice was assessed 30 minutes after the intraperitoneal injection of 5.0mg/kg Clozapine N-Oxide
718 (CNO). Following the behavioral tests, the mice underwent intracardial perfusion with 0.9% NaCl for 30
719 seconds and 4% paraformaldehyde for 5 minutes. Individual brains were dissected, fixed with 4% PFA for
720 12 hours, and subsequently dehydrated with 30% sucrose for 24 hours. The brains were then coronally
721 sliced into 20μm sections using a cryostat (Figure S5) (Pinskiy et al., 2013).

722 For the two-photon imaging experiments, a total of 300nl pAAV9-hSyn-GCamp6f-WPRE-hGHpA
723 ($1\times10^{13} GC/ml$) virus was injected into the PPC in the right hemisphere (Keiser et al., 2018). Post-virus
724 injection, a small window of 300μm to 400μm in diameter was drilled just above the PPC and covered with
725 a 1mm-high slide. The mice were allowed a two-week recovery period before the two-photon imaging
726 experiments. An imaging baseplate was positioned over the slide and secured with dental acrylic. Fast
727 high-resolution miniature two-photon microscopy (FHIRM-TPM) was employed, and its holder was mounted
728 onto the baseplate. Images were simultaneously acquired at a predetermined frame rate during the
729 behavior tests.

730 **Novel object recognition test**

731 The Novel Object Recognition (NOR) test was conducted to examine the integrity of an animal's visual
732 sensory input (Antunes and Biala, 2012), which consisted of three distinct phases (Figure S6). In Phase 1
733 (P1), each mouse was allowed to freely explore an empty arena for 10 minutes to acclimate to the
734 environment. In Phase 2 (P2), two identical objects (green cylinders) were placed at opposite corners of
735 the arena, and the mice were given another 10 minutes to explore. In Phase 3 (P3), one of the familiar
736 objects was replaced with a novel object (a yellow cube), and the mice were again provided 10 minutes to
737 explore the arena. The analysis of the mice's exploratory behavior and the calculation of the PI followed a
738 protocol similar to that used in the olfactory test. A positive PI value during P3 indicated a preference for
739 the novel object.

740 **Two-photon imaging processing**

741 Images of neuronal activities in the PPC layer II/III were captured in freely moving mice using FHIRM-TPM
742 microscopy at a resolution of 600×512 pixels (487.80×416.20μm) and a frame rate of 10Hz (Figure 2B).
743 The two-photon images were processed using established protocols, including motion correction, noise
744 reduction, and segmentation of neuronal components (de Vries et al., 2020; Giovannucci et al., 2019; Lecoq
745 et al., 2021; Pnevmatikakis and Giovannucci, 2017). For motion correction, the NoRMCorre algorithm was
746 employed to compensate for rigid and non-rigid translational movement (Pnevmatikakis and Giovannucci,
747 2017). Specifically, a reference frame with most activated neurons was manually selected from a subset of
748 frames (one frame chosen from every 500, for a total of 60 frames). Each frame in the subset was aligned
749 to this reference. The aligned frames were then averaged to create an initial reference image for the
750 registration of the entire video. The mean projection images, both before and after registration, were
751 illustrated (Figure S8A and S8B). Furthermore, the DeepInterpolation method, based on an encoder-
752 decoder network with skip connections, was applied to reduce Poisson noise within individual frames
753 (Lecoq et al., 2021). The model, originally trained on high-frequency (30Hz) data, was fine-tuned using our
754 10Hz dataset, resulting in effective noise reduction (Figure S8C and S8D).

755 Segmentation of neuronal components was initially performed using established morphological methods
756 (de Vries et al., 2020). Briefly, the two-photon images were divided into blocks of 100 frames (Figure S8E).
757 For each block, both maximum and average intensity projections were calculated (Figure S8E). The
758 difference between these projections was subjected to an adaptive threshold filter to generate a periodic
759 mask containing multiple components (Figure S8E). These periodic masks were subsequently refined using
760 morphological operations, such as hole filling. Subsequently, we developed a new strategy to integrate
761 these periodic masks and automatically identify individual neuronal components. We observed that pixels
762 belonging to the same neuronal structure were more likely to be consistently grouped into the same
763 component across different periodic masks, providing a basis for identifying all pixels within a given
764 neuronal component. Specifically, for any given pair of pixels, the Jaccard Index (JI) was calculated as the
765 ratio of the number of blocks in which both pixels were classified into the same component to the number
766 of blocks in which either pixel was identified in any component (Jaccard, 1901). Pixels with a JI value of 0.5
767 or higher were grouped together, representing the spatial footprint of different regions of interest (ROI).
768 Consequently, a temporal mask was generated (Figure S8F). To address potential ROI overlap, which may
769 arise from a single neuron or from distinct neurons sharing similar imaging fields, we calculated the

770 percentage of pixel pairs with a JI greater than 0.5 between two ROIs. A threshold of 80% or higher was
771 used to determine whether the two ROIs originated from the same neuron. Overlapping areas were then
772 merged to generate a spatial mask (Figure S8G). This spatial mask was further refined using the signal
773 quality of individual ROIs to generate a soma mask (Figure S8H). This process resulted in the identification
774 of three distinct soma-like components, which were defined as individual neurons (Figure S8I).

775 **Extraction of neuronal fluorescence signal**

776 Similar to the processing of two-photon images, neuronal signal extraction also followed established
777 protocols (de Vries et al., 2020; Kerr et al., 2005; Komiyama et al., 2010). Briefly, the initial fluorescence
778 signal of any given ROI in the spatial mask was calculated by the mean intensity of all associated pixels in
779 each frame (Figure S9A and S9B). The neuropil fluorescence was estimated by averaging the intensities
780 of an equivalent number of surrounding pixels (Figure S9A and S9B). An ROI was selected as neuron if its
781 fluorescence signal exceeded the 3-sigma level of its neuropil for at least three consecutive frames (Figure
782 S9B). The fluorescence signal was further refined by subtracting neuropil contamination and removing
783 polynomial trend. Next, a baseline filter was applied to normalize the fluorescence signal (Figure S9C and
784 S9D). This process resulted in the calcium signal, expressed as $\Delta F/F$, where ΔF represents the
785 fluorescence change from the baseline (Figure S9E). In the calcium signal, positive or negative transients
786 were identified by isolating segments of the signal that exceeded the baseline by more than two-sigma and
787 persisted for a minimum duration of three consecutive frames (Komiyama et al., 2010). The sigma value
788 was determined separately: for positive transients, using measurements below the baseline; for negative
789 transients, using measurements above the baseline (Dombeck et al., 2007; Komiyama et al., 2010).
790 Neurons exhibiting a positive-to-negative transient ratio greater than ten were selected for further analysis.
791 Finally, the event signal was extracted from the calcium signal, which was based on a frame rate of 100ms
792 and a decay constant (τ) of 860ms (Kerr et al., 2005).

793 **Quantity discrimination decoding analysis**

794 We conducted a detailed analysis of various neuronal features to decode the quantity discrimination
795 behavior in mice. These features were calculated for either individual neurons or neuronal population within
796 the PPC as described below. Notably, neurons located at the edges of the image were excluded to ensure
797 accurate decoding.

798 ***Neurons with preferential activities:*** We measured the activities of individual neurons when the animal
799 was located in the foraging zone for the specific amount of food. Specifically, the average firing magnitude
800 (FM) and the average firing rate (FR) per frame were assessed for each neuron. For animals presented
801 with a specific amount of food, the neurons with preferential activities (FM or FR) were identified at a given
802 time throughout the 60 min observation period (Figure S10). To determine whether preferential activities
803 changed over time, we tracked the identities of the individual neurons and their preferential activities across
804 time and compared the data between the beginning and ending halves. In 26 out of the 48 animals, all
805 neurons changed preferential activities. Overall, changed preferential activities were detected in 7,234 out
806 of the 7,378 recorded neurons (Figure 2D, 2E, and S11).

807 ***Synchronous firing of the PPC neuronal population:*** Among all the fired neurons in each animal
808 presented with a given amount of food, the average percentage of the neurons fired in the same frame or
809 the level of synchronous firing was calculated (Table 1, Figure S15). For the duration of synchronous firing,
810 the Jaccard Index (JI) similarity value greater than 0.7 in all the consecutive frames or more than 82% the
811 same neurons fired in all the consecutive frames were used for calculation (Figure 3A, S13) (Jaccard, 1901).

812 ***Similarity Index:*** To calculate whether the synchronous firing resulted from the participation of all the PPC
813 neurons or a selected group of the PPC neurons, the Similarity Index (SI) for the fired neurons in different
814 frames were analyzed (Figure S14).

815

Neural Entropy

Claude Shannon developed Shannon Entropy (*H*) to calculate the information content (Shannon, 1948). Given a variable X, with possible outcomes $x_1,...,x_s$, which occur with probability $p(x_1),...,p(x_s)$, the Shannon Entropy of X is defined as:

$$H(X)=\sum_{i=1}^{s} p(x_i)\log_2^{1/p(x_i)}$$

Shannon Entropy for a single transistor

A transistor on a computer chip has on and off statuses, which store information content following Shannon Entropy, as given by:

$$H(M)=\sum_{i=1}^{2} p(M_i)\log_2^{1/M_i}=\frac{1}{2}\log_2^2+\frac{1}{2}\log_2^2=1$$

Shannon Entropy for a population of transistors

A population of transistors on a computer chip constitutes a binary coding system (Hopfield, 1982), for which the information content can be expressed as the aggregate of the Shannon Entropy across S transistors in use, as calculated by:

$$H=\sum_{M=1}^{S}\sum_{i=1}^{2} p(M_i)\log_2^{1/p(M_i)}$$

For instance, for encoding a 20-pixels or 80-pixels gray image, the corresponding Shannon Entropy value would be 160 bits or 640 bits, respectively (Figure 4A).

Information Entropy for a single neuron

A neuron also has binary conditions of fire or rest. Given a neuron (N), with its firing frequency $p(N_1)$ and its resting frequency $p(N_2)$, its information content could be similarly calculated by:

$$H(N)=\sum_{i=1}^{2} p(N_i)\log_2^{1/p(N_i)}$$

Information Entropy for a pair of neurons

For a pair of neurons, they could fire synchronously or not (Figure 4B). Joint Entropy is employed to quantify the information content for associated events (Quian Quiroga and Panzeri, 2009). The Information Entropy for a pair of neurons (N,M) could be calculated by:

$$H(N,M)=\sum_{j=1}^{2}\sum_{i=1}^{2} p(N_j,M_i)\log_2^{1/p(N_j,M_i)}$$

Neural Entropy for a population of neurons

For a population of neurons or a brain region, it could code information by the levels of synchronous firing of the neurons. The information content could be calculated by the level of synchronous firing or pair-wise firing of the neurons in the population, termed as Neural Entropy (*N*). For a brain region performing a

845 particular task (X), it has a S number of neurons in its population and the pairs of synchronous firing
846 neurons (C_S^2). The information content could be calculated by measuring the level of synchronous firing or
847 the average of the aggregated pair-wise firing, the Neural Entropy:

848 $$N(X) = \frac{p(X)}{C_S^2} \sum_{N=1}^{S-1} \sum_{M=N+1}^{S} H(N,M)$$

849 For instance, for presented with either a 20g or 80g of food, the corresponding Neural Entropy value would
850 be 0.14 bits or 0.45 bits, respectively (Figure 4B and S16).

851 **QUANTIFICATION AND STATISTICAL ANALYSIS**

852 In our study, we employed various statistical methods to analyze the data, including the paired t-test, the
853 unpaired t-test, the one-way ANOVA, and the Mann-Whitney U test. P-values from the Mann-Whitney U
854 test were adjusted using the Benjamini-Hochberg method. P-values were reported using scientific notation
855 and rounded to two decimal places. In our data presentation, we utilized a variety of graphical
856 representations to effectively convey our findings. Specifically, bar graphs were employed to illustrate mean
857 values accompanied by Standard Error of the Mean (SEM) as error bars, with individual data points
858 represented as dots for clarity (*e.g.*, Figure 1D). Additionally, violin plots were utilized to display mean
859 values along with the interquartile range (25%-75%), providing insight into the distribution of the data. The
860 data distribution was further visualized using a kernel density estimate curve (*e.g.*, Figure S15). Moreover,
861 a specific graph was used to illustrate the distribution of the original data, presented through median values
862 and interquartile ranges (*e.g.*, Figure 3B).